Antiparticle of exciton in semimetals

Lingxian Kong, Ryuichi Shindou,[*] and Yeyang Zhang[†]

International Center for Quantum Materials, School of Physics, Peking University, Beijing 100871, China

An emergent quantized field enriches quantum many-body systems. We propose an antiparticle analog of the exciton in semimetals as an emergent collective mode in interacting electron systems. We show that interband excitations in semimetals are generally comprised of both excitons and antiparticles of excitons. These two stand for two distinct interband collective modes in semimetals, having different energies and opposite conserved charges. The conserved charge here is a quantity conjugate to a joint U(1) symmetry of two electrons' bands associated with the interband excitations. The opposite charges foster fertile scattering processes among the interband collective modes. In spin-polarized systems, they also suggest possible experimental detections of the antiparticles. We clarify that the effective theory of the interband excitations is given by a generalized Klein-Gordon theory. Our theory provides a comprehensive understanding of excitonic spectra in generic semimetals, bringing broader insight into electronic collective phenomena in solids.

I. INTRODUCTION

The existence of antiparticles is one of the most striking predictions by the quantum field theory [1]. It renews the basic concept of particles by showing that particle numbers are no longer conserved quantities. In elementary particle physics, every particle has a corresponding antiparticle in some forms. Some particles are their own antiparticles, such as photons and Higgs bosons, while others are not, such as electrons and quarks [2]. A pair of a particle and an antiparticle can be simultaneously created and/or annihilated. A typical example is an annihilation of an electron-positron pair producing two photons.

Electromagnetic and optical properties of solid-state materials are related to emergent collective modes in quantum many-particle systems of electrons and cations. Energy scales of the collective modes are typically much lower than those in high-energy experiments, while effective field theories of the emergent degrees of freedom often share rich mathematical structures with elementary particles in high-energy physics. Thus, it is an important quest to find collective modes in condensed matter systems as analogs of antiparticles.

In this paper, we demonstrate universal presence of the antiparticle analogs of excitons that are distinguishable from their counterpart excitons and that coexist with the counterpart excitons (see Fig. 1 and Fig. 2). In semiconductors, an exciton is a nonrelativistic boson that describes a bound state of a conduction-band electron and a valance-band hole. The bound state is an eigenstate of a two-body Hamiltonian of the electron and hole that interact through the long-range Coulomb interaction [3–5]. Excitons play crucial roles in optoelectronic properties in semiconductors [6–8]. In semimetals or narrow-gap semiconductors where the conduction and valance bands overlap or nearly overlap, excitons may undergo Bose-Einstein condensation [9–13]. The condensates are described by a Ginzburg-Landau theory as in superconductivity [14–16]. There is no antiparticle analog in such conventional theories of excitons.

There were attempts to define an antiparticle of the exciton [17–21]. Excitonic spectra in the condensates [20] or under external pumps [17,18] which induce a hopping between the conduction and valence bands have been studied previously. Thereby, the two-body Hamiltonian has pairs of degenerate positive- and negative-energy eigenstates [3,4,17,18], which are related to each other by a generic particle-hole symmetry of the Hamiltonian. They are sometimes dubbed as pairs of "exciton" and "antiexciton", respectively, in the literature [17,18], while such pairs of "two" states actually characterize identical physical excitations (see Appendix B). Besides, interband excitations in semiconductors with positive and "negative" band gaps are characterized as excitons and antiexcitons in other literature [20,21], while coexistence of these two kinds of interband collective modes in the same bulk has not been explored (Appendix B).

To reveal the coexistence of the exciton and the antiparticle of the exciton as two distinguishable collective modes in semimetals, we solve the Bethe-Salpeter (BS) equation for a two-band model with screened Coulomb interaction in two and three dimensions (Fig. 1 and Fig. 2). An interband two-particle Green's function obtained from the BS equation has a pair of *two* poles for the 1s exciton levels (1s hydrogen-atom-type orbitals for the relative coordinates between an electron and a hole). The inverse of the two-particle Green's function plays a role of the Lagrangian of free excitons [4]. The Lagrangian takes the form of a generalized Klein-Gordon field theory without the Lorentz symmetry. By quantizing the effective field theory [1], we show that the pair of the poles can be interpreted as an exciton and an antiparticle of the

---

[*]Corresponding author: rshindou@pku.edu.cn
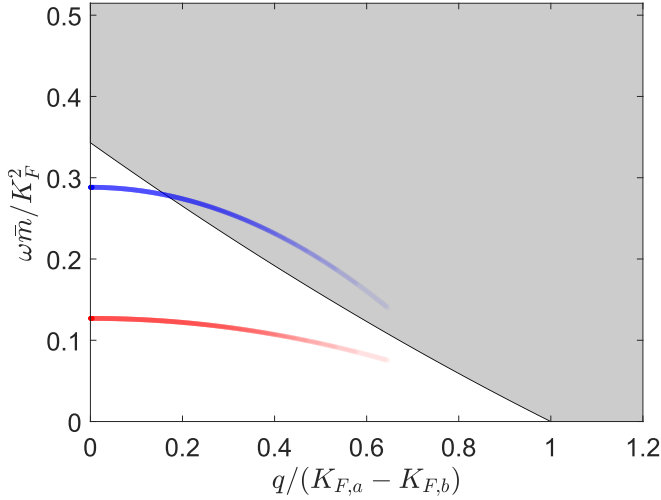[†]Corresponding author: yeyzhang@pku.edu.cn

235145-1

FIG. 1. Energy-momentum (ω-q) dispersions of the s-wave exciton (the red line) and antiexciton (the blue line) bands together with an energy-momentum region of interband individual excitations (the shaded region) in a two-band model in three dimensions given by Eqs. (1)–(3). The momentum of the interband excitations is given by $\boldsymbol{q}$ for $\boldsymbol{k_c} = 0$. In the case of $\boldsymbol{k_c} \neq 0$, the momentum $\boldsymbol{Q}$ of the interband excitations is given by $\boldsymbol{Q} = \boldsymbol{q} + \boldsymbol{k_c}$. The parameters set in this figure are the same as in Fig. 5(a). In this paper, the energy dispersions are always calculated perturbatively in small q around the Γ point. To emphasize this point, we use more transparent colors for the dispersions with larger q in this figure and other figures below.

FIG. 2. (a) A two-band semimetal model with $k_c \neq 0$. (b) A semimetal with $k_c = 0$. In a ground state, the conduction band (a band) and valence band (b band) have N_a and N_b electrons, respectively. $K_{F,a}$ and $K_{F,b}$ denote the Fermi momentum of a circular electron pocket in the a band and the Fermi momentum of a circular hole pocket in the b band. (c, d) Two types of interband collective modes in the semimetal with the U(1) × U(1) symmetry. (c) Exciton, an interband collective mode in the space of $|N_a + 1, N_b - 1\rangle$. A wave function of an exciton state has a weight mainly in a region of $|k| > K_{F,a}$. (d) Antiexciton, an interband collective mode in the space of $|N_a - 1, N_b + 1\rangle$. A wave function of an exciton state has a weight mainly in a region of $|k| < K_{F,b}$.

exciton (*antiexciton*), respectively. A calculation of conserved charge of the effective field theory shows that the exciton and antiexciton carry opposite charges, where the conserved charge is conjugate to a joint U(1) phase of the two bands. The opposite charge enables pair annihilation of an exciton and an antiexciton which produces a pair of density waves in conduction and valence bands. When the two bands have opposite spin polarization, e.g., one band with up-spin polarization ($s_z = 1/2$) and the other band with down-spin polarization ($s_z = -1/2$), the exciton and antiexciton carry $S_z = +1$ and $S_z = -1$. The opposite spin polarization can be utilized for distinguishing antiexcitons from excitons experimentally in the spin-polarized case.

The organization of this paper is as follows. In the next section, we introduce model Hamiltonians for semimetals studied in this paper. In Sec. III, we introduce the concept of the antiexciton in semimetals in terms of an interband two-particle Green's function. In Sec. IV, we explain how we calculate the Green's function in a limit of dilute carrier densities. In Sec. V, we demonstrate universal coexistence of exciton and antiexciton states based on calculations of energy-momentum dispersions of the interband collective modes. In Sec. VI, we show that a "CP-violated" Klein-Gordon theory describes a pair of an exciton and an antiexciton. In Sec. VII, we discuss possible optical spectroscopy experiments for detecting the antiexciton states in semimetals. A brief summary and relevant experimental materials are listed in Sec. VIII. In Appendix A, we provide technical details for calculations of the energy-momentum dispersion of exciton and antiexciton states in the semimetals. In Appendix B, we clarify the phys-
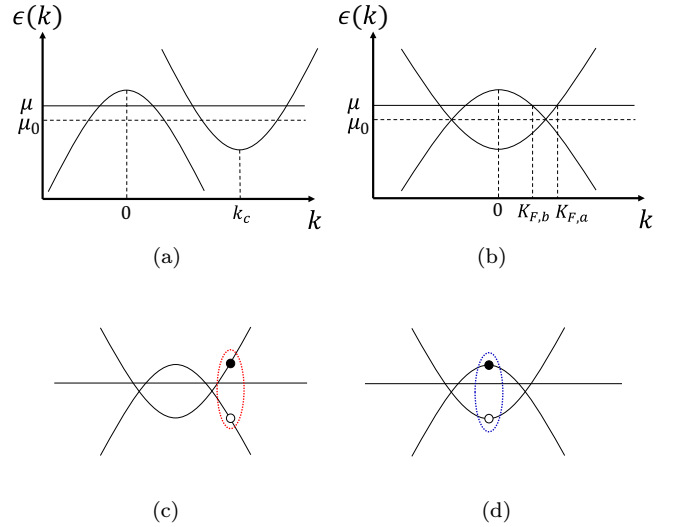
ical difference between our concept of the antiexciton and those in the literature [17–21].

II. MODELS OF SEMIMETALS

We study a two-band semimetal Hamiltonian with a valence-band maximum at $\boldsymbol{k} = 0$ and a conduction-band minimum at $\boldsymbol{k} = \boldsymbol{k_c}$ [Figs. 2(a) and 2(b)] [14,22]. The kinetic energy part of the electronic Hamiltonian is given by

$$\hat{K}_0 = \sum_{\boldsymbol{k}} [(\epsilon_a(\boldsymbol{k}) - \mu)a_{\boldsymbol{k}}^\dagger a_{\boldsymbol{k}} + (\epsilon_b(\boldsymbol{k}) - \mu)b_{\boldsymbol{k}}^\dagger b_{\boldsymbol{k}}] \quad (1)$$

with

$$\epsilon_a(\boldsymbol{k}) = \frac{k^2}{2m_a} + \frac{E_g}{2}, \quad \epsilon_b(\boldsymbol{k}) = -\frac{k^2}{2m_b} - \frac{E_g}{2}. \quad (2)$$

Here m_a and m_b are effective masses of a and b bands, respectively. The reduced Planck constant $\hbar$ is set to 1. E_g is an energy difference between the a-band energy minimum and the b-band energy maximum. E_g is negative for the semimetal case. We define $a_{\boldsymbol{k}}^\dagger$ and $a_{\boldsymbol{k}}$ as creation and annihilation operators for electrons of the conduction band with wave vector $\boldsymbol{k} + \boldsymbol{k_c}$, and define $b_{\boldsymbol{k}}^\dagger$ and $b_{\boldsymbol{k}}$ for electrons of the valence band with wave vector $\boldsymbol{k}$. A charge neutrality (the electron density equals the hole density) can be realized by a chemical potential of $\mu_0 = \frac{E_g(m_a - m_b)}{2(m_a + m_b)}$. To study the interband bound states with their crystal momenta $\boldsymbol{Q}$ around $\boldsymbol{k_c}$, we put the chemical potential away from the charge neutrality point, $\mu \neq \mu_0$, where interband electron-hole individual excitations have a finite gap at

$Q = k_c$ (see Fig. 1 and Fig. 2 with $Q = q + k_c$). The radii of the circular Fermi surface of a and b bands are denoted as $K_{F,a}$ and $K_{F,b}$ ($K_{F,a} \neq K_{F,b}$). For clarity of presentation, we put $k_c = 0$ ($Q = q$), and choose $\mu > \mu_0$ ($K_{F,a} > K_{F,b}$) henceforth. The following argument can be directly applied to the case of $k_c \neq 0$ [14].

Electrons in the two bands interact through the long-range Coulomb interaction. The interaction takes the following form in the momentum representation:

$$\hat{V} = \frac{1}{2\Omega} \sum_q v(q) \hat{\rho}(q) \hat{\rho}(-q), \quad (3)$$

with a total volume of the system Ω. Here $\hat{\rho}(q)$ stands for the density operator with momentum q [14,22],

$$\hat{\rho}(q) = \sum_k (a^\dagger_{k+q} a_k + b^\dagger_{k+q} b_k), \quad (4)$$

and $v(q)$ is the Fourier transform of the bare Coulomb potential,

$$v(q) = \begin{cases} \frac{4\pi}{q^2} & \text{in three dimensions} \\ \frac{2\pi}{q} & \text{in two dimensions.} \end{cases} \quad (5)$$

The elementary charge e and the Coulomb constant $(4\pi\epsilon_0)^{-1}$ are set to 1. Since the Hamiltonian, $\hat{K}_0 + \hat{V}$, has no single-particle interband hopping terms, the interacting model has a $U(1) \times U(1)$ symmetry.

III. EXCITON AND ANTIEXCITON IN SEMIMETALS

Suppose that a many-body ground state $|0\rangle$ of the interacting electron system does not break the $U(1) \times U(1)$ symmetry. Therefore, it is in the eigenspace of total particle-number operators of a- and b-band electrons, $|N_a, N_b\rangle$, where N_a and N_b denote the electron numbers in a and b bands, respectively. Then, the interband excited eigenstates in the semimetals can be either in $|N_a + 1, N_b - 1\rangle$ or in $|N_a - 1, N_b + 1\rangle$. Excitons and antiexcitons are nothing but bound states living in the former and latter eigenspaces, respectively. These excitations can be characterized by a time-ordered interband two-particle Green's function in the zero-temperature ($T = 0$) field theory:

$$G^{ex}(x - x', t - t')_{yy'}$$
$$= -(-i)^2 \langle 0| \mathcal{T}\{a_x(t) b^\dagger_{x+y}(t) b_{x'+y'}(t') a^\dagger_{x'}(t')\} |0\rangle. \quad (6)$$

Here the many-body ground state $|0\rangle$ is in the $|N_a, N_b\rangle$ Hilbert space. $\mathcal{T}$ denotes the time-ordered product [23]. a_x and b_x are annihilation operators in the a and b bands. a_k and b_k in Eq. (1) are Fourier transforms of a_x and b_x,

$$a_x = \frac{1}{\sqrt{\Omega}} \sum_k e^{ikx} a_k, \quad b_x = \frac{1}{\sqrt{\Omega}} \sum_k e^{ikx} b_k, \quad (7)$$

with a total volume of the system Ω. y and y' in Eq. (6) are relative distances between the particle and hole that form a bound state. $x + \frac{m_b}{m_a + m_b} y$, $x' + \frac{m_b}{m_a + m_b} y'$ can be regarded as the center-of-mass coordinates of the particle and hole. The

Fourier transform of the two-particle Green's function is defined by

$$G^{ex}(q, \omega)_{kk'} = \int d(t - t') \int d^d(x - x') \int d^d y \int d^d y'$$
$$\times e^{i\omega(t - t') - iq \cdot (x - x') + ik \cdot y - ik' \cdot y'}$$
$$\times G^{ex}(x - x', t - t')_{yy'}. \quad (8)$$

In the semimetals, a spectral representation of the zero-temperature time-ordered Green's function for the interband excitations can be decomposed not only by the excited eigenstates in $|N_a + 1, N_b - 1\rangle$ but also by those in $|N_a - 1, N_b + 1\rangle$ as

$$G^{ex}(q, \omega)_{kk'} = \sum_n \frac{i\Omega \langle 0| b^\dagger_k a_{q+k} |n\rangle \langle n| a^\dagger_{q+k'} b_{k'} |0\rangle}{\omega - (E_n - E_0) + i0^+}$$
$$- \sum_{n'} \frac{i\Omega \langle 0| a^\dagger_{q+k'} b_{k'} |n'\rangle \langle n'| b^\dagger_k a_{q+k} |0\rangle}{\omega + (E_{n'} - E_0) - i0^+}. \quad (9)$$

Here E_0 is a ground-state energy in the $|N_a, N_b\rangle$ Hilbert space. q and ω correspond to the total momentum and frequency of the interband bound states, and k, k' are relative momenta. $|n\rangle$ and $|n'\rangle$ are the excited eigenstates with the momentum q and $-q$ and with the energy E_n and $E_{n'}$ in the eigenspaces of $|N_a + 1, N_b - 1\rangle$ and $|N_a - 1, N_b + 1\rangle$, respectively. Excitons and antiexcitons are bound states comprised of interband excitations in $|N_a + 1, N_b - 1\rangle$ and $|N_a - 1, N_b + 1\rangle$, respectively. In the spectral representation, they can be detected as poles in the fourth and second quadrants in the complex-ω plane, respectively.

In a semiconductor with $E_g > 0$, $N_a = 0$, and $N_b = N$, the interband excited eigenstates are only in the space of $|1, N - 1\rangle$, where there is no antiparticle-type exciton. Lerner and Lozovik previously studied interband collective modes in two-dimensional (2D) electron-hole gas (EHG) under magnetic field and described the collective modes in two different field regimes as excitons and antiexcitons, respectively [20]. The 2D EHG under the field can approximately realize its ground states either in the space of $|0, N\rangle$ (positive-band-gap semiconductor regime) or in the space of $|N, 0\rangle$ (negative-band-gap semiconductor regime). Interband collective modes in these two semiconductor regimes live in $|1, N - 1\rangle$ and in $|N - 1, 1\rangle$, which can be also regarded as excitons and antiexcitons, respectively [20] (see Appendix B).

IV. SEMIMETALS WITH DILUTE CARRIER DENSITIES

In the dilute limit of the carrier densities, the two-particle Green's function can be evaluated in terms of the ladder approximation represented by the Feynman diagram in Fig. 3 [23],

$$G^{ex}(x - x', t - t')_{yy'}$$
$$= G^{ex}_0(x - x', t - t')_{yy'}$$
$$+ i \int d^d \bar{x} \int d^d \bar{y} \int d\bar{t} \; G^{ex}_0(x - \bar{x}, t - \bar{t})_{y\bar{y}}$$
$$\times w(\bar{y}) G^{ex}(\bar{x} - x', \bar{t} - t')_{\bar{y}y'}, \quad (10)$$

FIG. 3. The Feynman diagram of the screened-ladder approximation for G^{ex}. The upper and lower solid lines with rightward and leftward arrows are electron propagators in the b band and a band, respectively. The double wavy line is the screened Coulomb interaction $w(\boldsymbol{y})$ or $w(\boldsymbol{k} - \boldsymbol{k}')$ represented by the Feynman diagram in Fig. 4.

where $G_0^{ex}(\boldsymbol{x} - \boldsymbol{x}', t - t')_{yy'}$ denotes the two-particle Green's function in a free theory ($V = 0$),

$$
G_0^{ex}(\boldsymbol{x} - \boldsymbol{x}', t - t')_{yy'} = G_0^a(\boldsymbol{x} - \boldsymbol{x}', t - t')
$$
$$
\times G_0^b(\boldsymbol{x}' - \boldsymbol{x} + \boldsymbol{y}' - \boldsymbol{y}, t' - t). \quad (11)
$$

Here G_0^a and G_0^b are single-particle Green's functions of the a and b bands in the free theory, respectively,

$$
iG_0^a(\boldsymbol{x} - \boldsymbol{x}', t - t') \equiv \langle 0|\mathcal{T}\{a_{\boldsymbol{x}}(t)a_{\boldsymbol{x}'}^\dagger(t')\}|0\rangle_{|V=0}, \quad (12)
$$

$$
iG_0^b(\boldsymbol{x} - \boldsymbol{x}', t - t') \equiv \langle 0|\mathcal{T}\{b_{\boldsymbol{x}}(t)b_{\boldsymbol{x}'}^\dagger(t')\}|0\rangle_{|V=0}. \quad (13)
$$

Their Fourier transforms are as follows:

$$
G_0^{ex}(\boldsymbol{q}, \omega)_{kk'} = \Omega\delta_{kk'} \int \frac{d\omega_1}{2\pi} G_0^a(\boldsymbol{k} + \boldsymbol{q}, \omega_1 + \omega) G_0^b(\boldsymbol{k}, \omega_1)
$$
$$
= i\Omega\delta_{kk'} \left\{ \frac{\theta(|\boldsymbol{k} + \boldsymbol{q}| - K_{F,a})\theta(|\boldsymbol{k}| - K_{F,b})}{\omega - [\epsilon_a(\boldsymbol{k} + \boldsymbol{q}) - \epsilon_b(\boldsymbol{k})] + i0^+} \right.
$$
$$
\left. - \frac{\theta(K_{F,a} - |\boldsymbol{k} + \boldsymbol{q}|)\theta(K_{F,b} - |\boldsymbol{k}|)}{\omega - [\epsilon_a(\boldsymbol{k} + \boldsymbol{q}) - \epsilon_b(\boldsymbol{k})] - i0^+} \right\}, \quad (14)
$$

with

$$
G_0^a(\boldsymbol{k}, \omega) = \frac{\theta(|\boldsymbol{k}| - K_{F,a})}{\omega - \epsilon_a(\boldsymbol{k}) + i0^+} + \frac{\theta(K_{F,a} - |\boldsymbol{k}|)}{\omega - \epsilon_a(\boldsymbol{k}) - i0^+},
$$
$$
G_0^b(\boldsymbol{k}, \omega) = \frac{\theta(K_{F,b} - |\boldsymbol{k}|)}{\omega - \epsilon_b(\boldsymbol{k}) + i0^+} + \frac{\theta(|\boldsymbol{k}| - K_{F,b})}{\omega - \epsilon_b(\boldsymbol{k}) - i0^+}. \quad (15)
$$

Here $K_{F,a}$ and $K_{F,b}$ are the Fermi momenta of the circular Fermi surfaces of the conduction band and valence band, respectively [Fig. 2(b)]. $w(\boldsymbol{y})$ in Eq. (10) stands for an effective interaction between the electron and hole. In a semiconductor regime ($E_g > 0$), it is the long-ranged Coulomb interaction. In a semimetal regime ($E_g < 0$), the Coulomb interaction is screened by carrier densities. The screened Coulomb interaction can be evaluated by the random phase approximation (Fig. 4). In the approximation, the Fourier transform of $w(\boldsymbol{y})$ is given by a static limit of the bare polarization function
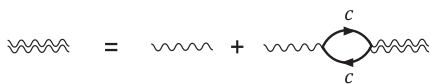

FIG. 4. Random phase approximation (RPA) for screened Coulomb interaction. The single- and double-wavy lines are bare (long-ranged) and screened Coulomb interactions. Solid lines of bubbles correspond to free single-particle Green's functions. A bubble with label c contains a summation of bubbles consisting of free single-particle Green's functions of the a and b bands ($c = a, b$).

$\Pi_0(\boldsymbol{q}, \omega)$,

$$
w(\boldsymbol{q}) = \frac{v(\boldsymbol{q})}{1 - v(\boldsymbol{q})\Pi_0(\boldsymbol{0}, 0)}
$$
$$
= \begin{cases} \frac{4\pi}{q^2 - 4\pi\Pi_0(\boldsymbol{0}, 0)} & \text{in three dimensions} \\ \frac{2\pi}{q - 2\pi\Pi_0(\boldsymbol{0}, 0)} & \text{in two dimensions.} \end{cases} \quad (16)
$$

The bare polarization function in our two-band model is given by

$$
\Pi_0(\boldsymbol{q}, \omega) = \sum_{c=a,b} \Pi_0^c(\boldsymbol{q}, \omega),
$$

$$
\Pi_0^c(\boldsymbol{q}, \omega) = -i \iint \frac{d\omega_1 d^d\boldsymbol{k}}{(2\pi)^{d+1}} G_0^c(\boldsymbol{k} + \boldsymbol{q}, \omega_1 + \omega) G_0^c(\boldsymbol{k}, \omega_1). \quad (17)
$$

The static limit of the polarization function is given by

$$
\Pi_0(\boldsymbol{0}, 0) \equiv \begin{cases} -\frac{1}{4\pi}\left(\frac{2K_{F,a}m_a}{\pi} + \frac{2K_{F,b}m_b}{\pi}\right) & \text{in three dimensions} \\ -\frac{1}{2\pi}(m_a + m_b) & \text{in two dimensions.} \end{cases} \quad (18)
$$

The screened Coulomb potential is given by the Thomas-Fermi (TF) wavelength k_{TF} as $w(\boldsymbol{k}) = 4\pi/(k^2 + k_{\text{TF}}^2)$ in three dimensions and $w(\boldsymbol{k}) = 2\pi/(k + k_{\text{TF}})$ in two dimensions. The TF wave vector is calculated as $k_{\text{TF}}^2 = 2(K_{F,a}m_a + K_{F,b}m_b)/\pi$ in three dimensions and $k_{\text{TF}} = m_a + m_b$ in two dimensions.

In the momentum-frequency space, Eq. (10) takes the form of

$$
\widetilde{G}^{ex}(\boldsymbol{q}, \omega)_{kk'} = \widetilde{G}_0^{ex}(\boldsymbol{q}, \omega)_{kk'} - \frac{1}{\Omega} \sum_{\boldsymbol{k}_1\boldsymbol{k}_2} \widetilde{G}_0^{ex}(\boldsymbol{q}, \omega)_{kk_1} w(\boldsymbol{k}_1
$$
$$
- \boldsymbol{k}_2)\widetilde{G}^{ex}(\boldsymbol{q}, \omega)_{k_2 k'}, \quad (19)
$$

with $i\Omega\widetilde{G}^{ex}(\boldsymbol{q}, \omega)_{kk'} \equiv G^{ex}(\boldsymbol{q}, \omega)_{kk'}$, $i\Omega\widetilde{G}_0^{ex}(\boldsymbol{q}, \omega)_{kk'} \equiv G_0^{ex}(\boldsymbol{q}, \omega)_{kk'}$. Equation (19) can be written into the following matrix form [4]:

$$
\widetilde{G}^{ex}(\boldsymbol{q}, \omega)^{-1} = \widetilde{G}_0^{ex}(\boldsymbol{q}, \omega)^{-1} + W, \quad (20)
$$

with $W_{kk'} \equiv \Omega^{-1}w(\boldsymbol{k} - \boldsymbol{k}')$. Suppose that $|\phi_j(\boldsymbol{q}, \omega)\rangle$ and $\xi_j(\boldsymbol{q}, \omega)$ are eigenvectors and eigenvalues of Eq. (20),

$$
\widetilde{G}^{ex}(\boldsymbol{q}, \omega)^{-1}|\phi_j(\boldsymbol{q}, \omega)\rangle = \xi_j(\boldsymbol{q}, \omega)|\phi_j(\boldsymbol{q}, \omega)\rangle. \quad (21)
$$

Then, the interband two-particle Green's function is given by the eigenvectors and eigenvalues,

$$
\widetilde{G}^{ex}(\boldsymbol{q}, \omega) = \sum_j |\phi_j(\boldsymbol{q}, \omega)\rangle\xi_j(\boldsymbol{q}, \omega)^{-1}\langle\phi_j(\boldsymbol{q}, \omega)|. \quad (22)
$$

In the next section, we solve Eq. (21) at $\boldsymbol{q} = 0$, where we can employ the spherical and circular symmetry in three and two dimensions, respectively, and use the irreducible representations of the symmetries. From $\xi_j(\boldsymbol{0}, \omega)$ thus calculated, we determine exciton and antiexciton levels at the Γ point. Then we treat small $\boldsymbol{q}$ around the Γ point as a perturbation and calculate band curvatures of the exciton and antiexciton bands, using the irreducible representations at $\boldsymbol{q} = 0$.

Before closing this section, let us use the Feynman-Hellman theorem and derive a useful relation between $\partial_\omega \xi_j$ and wave functions of exciton and antiexciton excitation at

$q = 0$. The ω derivative of Eq. (21) at the Γ point leads to

$$\frac{d\xi_j(\mathbf{0}, \omega)}{d\omega} = \langle \phi_j(\mathbf{0}, \omega)| \left[\frac{d\widetilde{G}^{ex}(\mathbf{0}, \omega)^{-1}}{d\omega} \right] |\phi_j(\mathbf{0}, \omega)\rangle, \quad (23)$$

where $\widetilde{G}^{ex}(\mathbf{0}, \omega)^{-1}$ and its ω derivate are given by

$$[\widetilde{G}^{ex}(\mathbf{0}, \omega)^{-1}]_{kk'} = \delta_{kk'} \left\{ \theta(|\mathbf{k}| - K_{\text{out}})\left(\omega - (\epsilon_a(\mathbf{k}) - \epsilon_b(\mathbf{k}))\right) - \theta(K_{\text{in}} - |\mathbf{k}|)\left(\omega - (\epsilon_a(\mathbf{k}) - \epsilon_b(\mathbf{k}))\right) \right\} + \frac{w(\mathbf{k} - \mathbf{k}')}{\Omega},$$

$$\left[\partial_\omega \widetilde{G}^{ex}(\mathbf{0}, \omega)^{-1} \right]_{kk'} = \delta_{kk'} \{ \theta(|\mathbf{k}| - K_{\text{out}}) - \theta(K_{\text{in}} - |\mathbf{k}|) \}. \quad (24)$$

Here $K_{\text{out}} \equiv \max(K_{F,a}, K_{F,b}) = K_{F,a}$, and $K_{\text{in}} \equiv \min(K_{F,a}, K_{F,b}) = K_{F,b}$. From this expression, we can relate the derivative with the momentum-space wave functions,

$$\partial_\omega \xi_j = \sum_{|\mathbf{k}| > K_{\text{out}}} |\langle \mathbf{k}|\phi_j\rangle|^2 - \sum_{|\mathbf{k}| < K_{\text{in}}} |\langle \mathbf{k}|\phi_j\rangle|^2, \quad (25)$$

with $K_{\text{out}} = K_{F,a} > K_{\text{in}} = K_{F,b}$.

As shown in the next section, $\xi_j(\mathbf{0}, \omega)$ as a function of ω crosses zero at both a positive ω ($\omega = \omega_+$) with $\partial_\omega \xi_j(\mathbf{0}, \omega)|_{\omega=\omega_+} > 0$ and a negative ω ($\omega = -\omega_-$) with $\partial_\omega \xi_j(\mathbf{0}, \omega)|_{\omega=-\omega_-} < 0$. The Lehmann representation dictates that the positive zero corresponds to a bound state in $|N_a + 1, N_b - 1\rangle$ (exciton) and the negative zero corresponds to a bound state in $|N_a - 1, N_b + 1\rangle$ (antiexciton). In fact, Eq. (25) shows that the eigenvectors of the positive-ω (negative-ω) bound states have larger spectral weight in $|\mathbf{k}| > K_{\text{out}}$ ($|\mathbf{k}| < K_{\text{in}}$), suggesting that the former and latter bound states are of $a_k^\dagger b_k|0\rangle$ type and of $b_k^\dagger a_k|0\rangle$ type, respectively [Figs. 2(c) and 2(d)].

V. ENERGIES OF INTERBAND EXCITATIONS IN SEMIMETALS

Solving Eq. (21) in three and two dimensions is computationally expensive for general q. Thus, we first focus on the solutions at $q = 0$. $G^{ex}(\mathbf{0}, \omega)$ has the spatially rotational symmetry,

$$G^{ex}(\mathbf{0}, \omega)_{kk'} = G^{ex}(\mathbf{0}, \omega)_{\widetilde{k}\widetilde{k}'}, \quad (26)$$

where $\widetilde{k}$ and $\widetilde{k}'$ are transformed into k and k', respectively, by the same rotation. The eigenvalue problem at the Γ point is decomposed by the irreducible representations of the rotational symmetry group (Appendix A). The Green's function is expanded by spherical harmonics in the 3D case,

$$-iG^{ex}(\mathbf{0}, \omega)_{kk'} = \sum_{nlm} \frac{Y_{lm}(\theta, \varphi) f_{nl}(\omega; k) f_{nl}(\omega; k') Y_{lm}^*(\theta', \varphi')}{\xi_{nl}(\omega)}, \quad (27)$$

and by trigonometric functions in the 2D case,

$$-iG^{ex}(\mathbf{0}, \omega)_{kk'} = \sum_{nm} \frac{f_{nm}(\omega; k) f_{nm}(\omega; k') e^{im(\varphi - \varphi')}}{\xi_{nm}(\omega)}. \quad (28)$$

Here $k = k(\sin\theta \cos\varphi, \sin\theta \sin\varphi, \cos\theta)$ in the 3D case and $k = k(\cos\varphi, \sin\varphi)$ in the 2D case. $f_{nl}(\omega; k)$ and $f_{nm}(\omega; k)$

stand for radial wave functions and $Y_{lm}(\theta, \varphi)$ are the spherical harmonics. In the 3D and 2D cases, $\langle \mathbf{k}|\phi_j(\mathbf{0}, \omega)\rangle = \frac{1}{\sqrt{\Omega}} f_{nl}(\omega; k) Y_{lm}(\theta, \varphi)$ and $\langle \mathbf{k}|\phi_j(\mathbf{0}, \omega)\rangle = \frac{1}{\sqrt{\Omega}} f_{nm}(\omega; k) e^{im\varphi}$, respectively. Here j is the combination of principal quantum number n, azimuthal quantum number l in the 3D case, and magnetic quantum number m in the 2D case.

Figure 5 plots $\xi_j(\mathbf{0}, \omega)$ as a function of ω. Individual interband excitations with $q = 0$ form continuum spectra in certain
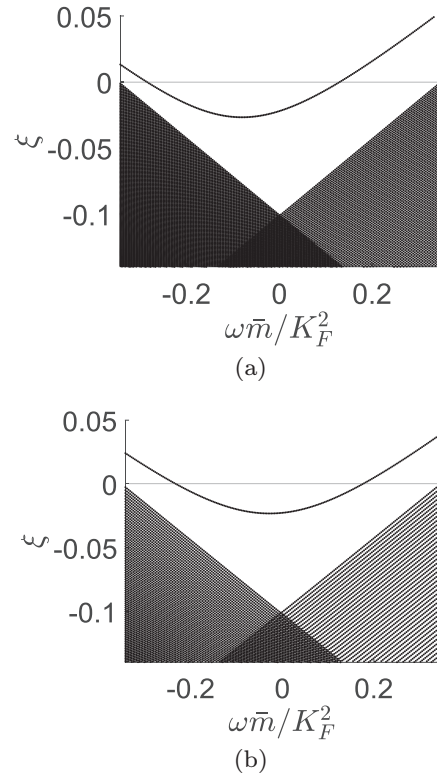

FIG. 5. $\xi_j(\mathbf{q} = \mathbf{0}, \omega)$ as a function of ω, with $m_a = m_b \equiv \bar{m}$, $K_F \equiv (K_{F,a} + K_{F,b})/2$. Locations of the zeros ($\xi_j(\mathbf{q} = \mathbf{0}, \omega) = 0$) are determined by three dimensionless quantities, $K_F \alpha_B$, $\tilde{E}_g \equiv E_g \bar{m}/K_F^2$, and $\tilde{\mu} \equiv \mu \bar{m}/K_F^2$, where the effective Bohr radius $\alpha_B = 1/\bar{m}$. The electron rest mass m_e is set to 1. (a) Three-dimensional (3D) case: eigenvalues with $l = 0$, $m = 0$ are plotted for $K_F \alpha_B = K_F/3.5 = 0.289$, $\tilde{E}_g = -0.3\bar{m}/K_F^2 = -1.03$, and $\tilde{\mu} = 0.05\bar{m}/K_F^2 = 0.172$. (b) 2D case: eigenvalues with $m = 0$ are plotted for $K_F \alpha_B = K_F = 0.540$, $\tilde{E}_g = -0.3\bar{m}/K_F^2 = -1.03$, and $\tilde{\mu} = 0.05\bar{m}/K_F^2 = 0.172$.
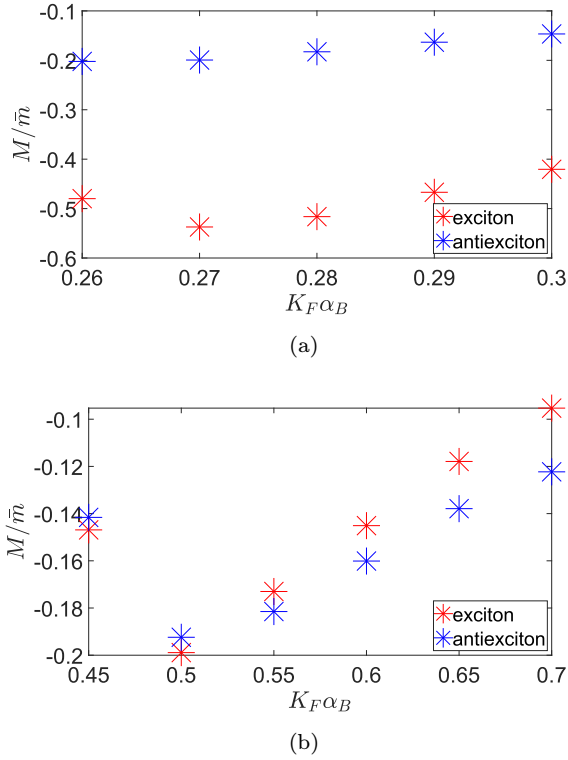
FIG. 6. Ratios between curvatures of the s-wave exciton and antiexciton bands and the mass of the electron and hole bands $\bar{m} \equiv m_a = m_b$. The ratios are plotted as a function of a dimensionless quantity $K_F \alpha_B$, where $K_F \equiv (K_{F,a} + K_{F,b})/2$ and $\alpha_B \equiv 1/\bar{m}$ (the effective Bohr radius of the electron system). The exciton's and antiexciton's band curvatures are defined in the expansion $\omega_\pm(\boldsymbol{q})$ around the Γ point, $\omega_\pm(\boldsymbol{q}) \equiv \omega_\pm + q^2/(2M)$. (a) The 3D case. (b) The 2D case. In these two plots, we choose $\tilde{E}_g = -1.03$ and $\tilde{\mu} = 0.172$.

ranges of ω, which correspond to the shaded regions in the figure. Apart from the continuum spectra, a branch of s-wave ($l = 0$) bound states in three dimensions and a branch of $m = 0$ bound states in two dimensions form a parabolic curve of ω outside the shaded region. The branch crosses zero at both a positive ω ($\omega = \omega_+$) and a negative ω ($\omega = -\omega_-$). The spectral representation dictates that the positive zero corresponds to a bound state in $|N_a + 1, N_b - 1\rangle$ (exciton) and the negative zero corresponds to a bound state in $|N_a - 1, N_b + 1\rangle$ (antiexciton). Energies of excitons and antiexcitons at finite $\boldsymbol{q}$ can be expanded as $\omega_\pm(\boldsymbol{q}) = \omega_\pm + q^2/(2M)$ to the lowest order in q. The band curvature $1/(2M)$ can be calculated from the irreducible representations of Eq. (20) (see Appendix A). In parameter ranges studied in this paper, the band curvatures always take negative values both for the exciton and antiexciton bands (Figs. 1 and 6). When energies of these interband bound states touch zero at finite $\boldsymbol{q}$ outside the energy-momentum region of the interband individual excitations, the system can undergo Bose-Einstein condensation. When the exciton or antiexciton condensates, the two bound-state modes become a Goldstone mode and a Higgs mode [24–27].

VI. EFFECTIVE FIELD INTERPRETATION

$\xi_j(\boldsymbol{0}, \omega)$ is an eigenvalue of the inverse of the interband two-particle Green's function $\widetilde{G}^{ex}(\boldsymbol{0}, \omega)^{-1}$. To the quadratic level in ω, it can be regarded as an effective Lagrangian for interband collective modes at $\boldsymbol{q} = 0$. Unlike in the semiconductor case, the ω-dependent part of the $\widetilde{G}^{ex}(\boldsymbol{0}, \omega)^{-1}$ matrix in the semimetal case is not simply proportional to an identity matrix. Namely, both of the terms on the right-hand side of Eq. (9) do not vanish in the semimetal case. Thus, $\xi_j(\boldsymbol{0}, \omega)$ becomes a nonlinear function of ω. The simplest effective Lagrangian for the interband collective excitations in semimetals contains an ω^2 term in addition to an ω term,

$$\xi_j(\boldsymbol{0}, \omega) = \gamma \omega^2 + \alpha \omega - \beta, \tag{29}$$

with $\gamma > 0$ and $\beta > 0$ (see Fig. 5). Thus, the effective Lagrangian contains a second-order time derivative of a complex scalar field $\varphi(t)$ for the $\boldsymbol{q} = 0$ interband collective modes,

$$\int dt \mathcal{L} = \int dt \varphi^\dagger(t)\left(-\gamma \partial_t^2 + i\alpha \partial_t - \beta\right)\varphi(t), \tag{30}$$

with the field defined by

$$\varphi(t) \equiv \sum_{\boldsymbol{k}} \int_{-\infty}^{+\infty} dt' \langle \boldsymbol{k} | \phi_j(\boldsymbol{0}, t - t') \rangle b_{\boldsymbol{k}}^\dagger(t') a_{\boldsymbol{k}}(t'). \tag{31}$$

Here we omit j indices in $\varphi(t)$ and in the effective Lagrangian. The complex field is decomposed into two real fields, φ_1 and φ_2, as $\varphi \equiv \varphi_1 + i\varphi_2$. Two conjugate momenta are introduced as $\pi_1 \equiv \frac{\partial \mathcal{L}}{\partial(\partial_t \varphi_1)}$ and $\pi_2 \equiv \frac{\partial \mathcal{L}}{\partial(\partial_t \varphi_2)}$. This leads to an effective Hamiltonian for the $\boldsymbol{q} = 0$ interband collective modes in semimetals as

$$\begin{aligned}
\mathcal{H} &= \pi_1 \partial_t \varphi_1 + \pi_2 \partial_t \varphi_2 - \mathcal{L} \\
&= \frac{1}{2\lambda}\left(\pi_1^2 + \pi_2^2\right) + \frac{1}{2}\lambda \eta^2 \left(\varphi_1^2 + \varphi_2^2\right) + \frac{\alpha}{2\gamma}(\pi_2 \varphi_1 - \pi_1 \varphi_2).
\end{aligned} \tag{32}$$

Here $\lambda = 2\gamma$, and $\eta = \sqrt{\frac{\alpha^2}{4\gamma^2} + \frac{\beta}{\gamma}}$. The Hamiltonian takes the form of two coupled harmonic oscillators and is bosonized by two boson fields:

$$\mathcal{H} = \nu_+ a_+^\dagger a_+ + \nu_- a_-^\dagger a_-, \tag{33}$$

with

$$a_{1,2} \equiv \sqrt{\frac{\lambda \eta}{2}}\left(\varphi_{1,2} + \frac{i}{\lambda \eta}\pi_{1,2}\right), \quad a_\pm \equiv \frac{1}{\sqrt{2}}(a_1 \pm ia_2), \tag{34}$$

and

$$\nu_\pm = \sqrt{\frac{\alpha^2}{4\gamma^2} + \frac{\beta}{\gamma}} \mp \frac{\alpha}{2\gamma}. \tag{35}$$

Note that, within the quadratic expansion of $\xi_j(\boldsymbol{0}, \omega)$ in ω, the two zeros of $\xi_j(\boldsymbol{0}, \omega)$ correspond to the quantized energies of the two bosons, $\nu_\pm = \omega_\pm(> 0)$. This concludes that a_+ and a_- boson operators represent the exciton and antiexciton annihilation operators, respectively. When $\alpha \neq 0$, the Hamiltonian describes two nondegenerate harmonic oscillators, whereas the Klein-Gordon theory (the $\alpha = 0$ case) describes two degenerate harmonic oscillators [1]. Thus, we can view the

interband collective modes in semimetals as a "*CP*-violated" Klein-Gordon field without the Lorentz symmetry.

Conserved charge

The Lagrangian in Eq. (30) is invariant under a U(1) transformation $\varphi \to \varphi e^{i\theta}$. By Noether's theorem, it has a conserved charge density [1,28]:

$$j^0 = -i\varphi \frac{\partial \mathcal{L}}{\partial(\partial_t \varphi)} + i\varphi^\dagger \frac{\partial \mathcal{L}}{\partial(\partial_t \varphi^\dagger)}$$

$$= i\gamma[\varphi^\dagger(\partial_t \varphi) - (\partial_t \varphi^\dagger)\varphi] + \alpha \varphi^\dagger \varphi. \quad (36)$$

From Eq. (34), φ is given by a linear combination of the annihilation of the exciton (a_+) and the creation of the antiexciton ($a_-^\dagger$):

$$\varphi = \frac{1}{\sqrt{\lambda\eta}}(a_+ + a_-^\dagger). \quad (37)$$

a_+ and a_- have their dynamical evolutions in the interaction picture for a quantum-mechanical problem: $a_+(t) = a_+ e^{-i\nu_+ t}$, $a_-(t) = a_- e^{-i\nu_- t}$. From Eqs. (36) and (37) together with the time evolutions, one can readily see that the density is time independent and is given by the difference between the exciton and antiexciton density:

$$j^0(t) = \frac{\gamma}{\lambda\eta}[(a_+^\dagger e^{i\nu_+ t} + a_- e^{-i\nu_- t})$$

$$\times (\nu_+ a_+ e^{-i\nu_+ t} - \nu_- a_-^\dagger e^{i\nu_- t}) + \text{H.c.}]$$

$$+ \frac{\alpha}{\lambda\eta}(a_+^\dagger e^{i\nu_+ t} + a_- e^{-i\nu_- t})(a_+ e^{-i\nu_+ t} + a_-^\dagger e^{i\nu_- t})$$

$$= \frac{\alpha + 2\gamma\nu_+}{\lambda\eta} a_+^\dagger a_+ + \frac{\alpha - 2\gamma\nu_-}{\lambda\eta} a_-^\dagger a_-$$

$$+ \frac{\gamma(\nu_+ - \nu_-) + \alpha}{\lambda\eta}[a_+^\dagger a_-^\dagger e^{i(\nu_+ + \nu_-)t} + \text{H.c.}]$$

$$= a_+^\dagger a_+ - a_-^\dagger a_-. \quad (38)$$

Here $\nu_\pm = \eta \mp \alpha/(2\gamma)$ and $\lambda = 2\gamma$. Thus, the particle a_+ carries charge $+1$, while the antiparticle a_- carries charge -1.

When the *a*-band and *b*-band electrons have an opposite physical property such as spin, the conserved charge carries the physical property. This is because a joint U(1) transformation, $a_k \to a_k e^{\frac{i\theta}{2}}$ and $b_k \to b_k e^{-\frac{i\theta}{2}}$, leads to $\varphi \to \varphi e^{i\theta}$ with $\varphi \propto b^\dagger a$. Suppose that the *a*-band electrons are with spin-up polarization along the *z* direction, and the *b*-band electrons are with spin-down polarization. Then exciton states carry $S_z = 1$ and antiexciton states carry $S_z = -1$. This can be also seen from the spectral representation of the Green's function, Eq. (9). In this case, spin-polarized excitation spectroscopy could distinguish exciton states from antiexciton states experimentally [29,30].

VII. PHYSICAL CONSEQUENCES

The antiexciton proposed in this paper represents a distinct interband collective excitation from its counterpart exciton having different energies ($\omega_+ \neq \omega_-$) and opposite physical charges. They manifest themselves as distinct peaks in optical spectroscopy experiments.
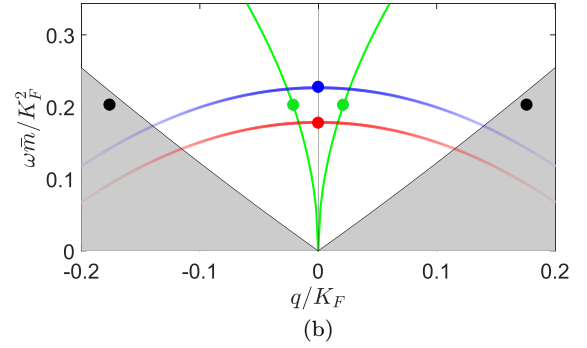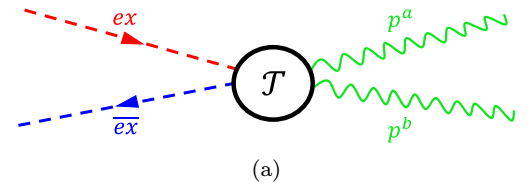

FIG. 7. (a) A conversion process between an exciton-antiexciton pair and intraband excitations. *ex* and $\overline{ex}$ stand for an exciton and an antiexciton, while p^a and p^b represent an intraband particle-hole excitation in the *a* and *b* bands, respectively. (b) Dispersions of the *s*-wave exciton (red) and antiexciton (blue) bands, plasmon band (green), and intraband individual excitations (the grey shaded area) around the Γ point in the 2D case for the same parameters as in Fig. 5(b). The pair of the $q = 0$ exciton and antiexciton (the red and blue points) can decay into (be created from) two intraband particle-hole excitations, which can be either individual excitations (the black points) or plasmons (the green points).

When a single interband excitation process by a photon is allowed by the symmetry and the charge dual to the joint U(1) phase, the optical spectroscopy experiment distinguishes the exciton and antiexciton from each other in the form of two distinct absorption peaks. When the direct excitation process is prohibited by the symmetry, an exciton-antiexciton pair can be excited by higher-order scattering processes. For example, in the eigenspace of $|N_a, N_b\rangle$, the energy-momentum conservation allows the pair to decay into two *intraband* collective or individual excitations [23,31] (Fig. 7), being analogous to the electron-positron pair annihilation that releases the two photons. The reverse process of the pair annihilation enables conversion from two photon-excited intraband excitations into an exciton-antiexciton pair.

Possible conversion processes of an exciton-antiexciton pair

The conversion between an exciton-antiexciton pair and multiple intraband collective excitations or individual excitations is constrained by the momentum and energy conservation and momentum-energy dispersions of the interband/intraband collective and/or individual excitations. In this section, we discuss the conversion process based on calculations of the momentum-energy dispersions of intraband and interband collective excitations around the Γ point for a specific set of parameters with $m_a = m_b = \bar{m}$, $\mu > 0$, and $K_{F,a} > K_{F,b}$.

In the presence of finite $K_{F,a}$ and $K_{F,b}$, individual excitations form continuum spectra on the ω-q plane. Borders of
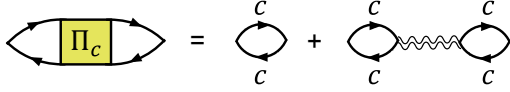
FIG. 8. Feynman diagrams of the RPA contributions to the polarization function $\Pi^c(\boldsymbol{q}, \omega)$ ($c = a$ or b). The double wavy lines represent screened Coulomb interactions given in Fig. 4. Solid lines with labels c stand for the free single-particle Green's functions of the c band ($c = a, b$).

the continuum spectra for the intraband individual excitations for the a and b bands are given by $\omega = (q^2 \pm 2K_{F,a}q)/(2m)$ and $\omega = (q^2 \pm 2K_{F,b}q)/(2m)$, respectively [31]. Intraband density-wave modes form momentum-energy dispersions outside the continuum spectra. The dispersion of the intraband density modes can be calculated from the polarization functions of the a-band and b-band densities,

$$\Pi_c(\boldsymbol{x} - \boldsymbol{x}', t - t')$$
$$= -i\langle 0| \mathcal{T}\{[\hat{\rho}^c(\boldsymbol{x}, t) - \rho_0^c][\hat{\rho}^c(\boldsymbol{x}', t') - \rho_0^c]\}|0\rangle. \quad (39)$$

Here $\hat{\rho}^c$ and ρ_0^c represent the c-band density operator and its ground-state average, respectively ($c = a, b$). Let $\Pi_c(\boldsymbol{q}, \omega)$ be the Fourier transform of $\Pi_c(\boldsymbol{x} - \boldsymbol{x}', t - t')$. In terms of the RPA, $\Pi^c(\boldsymbol{q}, \omega)$ is calculated as follows (Fig. 8):

$$\Pi^c(\boldsymbol{q}, \omega) = \Pi_0^c(\boldsymbol{q}, \omega) + \Pi_0^c(\boldsymbol{q}, \omega)w(\boldsymbol{q}, \omega)\Pi_0^c(\boldsymbol{q}, \omega),$$
$$w(\boldsymbol{q}, \omega) = \frac{v(\boldsymbol{q})}{1 - \Pi_0(\boldsymbol{q}, \omega)v(\boldsymbol{q})}, \quad (40)$$

where $\Pi_0^c(\boldsymbol{q}, \omega)$ and $\Pi_0(\boldsymbol{q}, \omega)$ are given by Eq. (17). Thus, the intraband density-wave modes for the two bands share the same denominator and the zeros of the denominator determine the momentum-energy dispersions of the plasmon mode,

$$1 - \Pi_0(\boldsymbol{q}, \omega)v(\boldsymbol{q}) = 0. \quad (41)$$

Using the Lindhard function at the limit of $q \to 0$ for three dimensions and $q \to 0, \omega \to 0$ for two dimensions [23,31,32],

$$\Pi_0^c(q, \omega) = \begin{cases} -\frac{m_c K_{F,c}}{4\pi^2}\left(2 - x_c \ln\left(\frac{x_c+1}{x_c-1}\right)\right) & \text{in three dimensions} \\ -\frac{m_c}{2\pi}\left(1 - \frac{|x_c|}{\sqrt{x_c^2-1}}\right) & \text{in two dimensions,} \end{cases} \quad (42)$$

with $x_c \equiv \frac{m_c \omega}{K_{F,c}q}$ ($c = a, b$), we further take $\omega \gg q$ and expand $\Pi_0(\boldsymbol{q}, \omega) \equiv \Pi_0^a(\boldsymbol{q}, \omega) + \Pi_0^b(\boldsymbol{q}, \omega)$ up to the fourth order of $\frac{1}{x_a}$ and $\frac{1}{x_b}$. Then we solve Eq. (41) for ω up to the subleading order in small q. This gives

$$\omega = \begin{cases} \sqrt{A_3}\left(1 + \frac{B_3}{2A_3^2}q^2\right) & \text{in three dimensions} \\ \sqrt{A_2 q}\left(1 + \frac{B_2}{2A_2^2}q\right) & \text{in two dimensions,} \end{cases} \quad (43)$$

with

$$A_3 = \sum_{c=a,b} \frac{2K_{F,c}^3}{3\pi m_c}, \quad A_2 = \sum_{c=a,b} \frac{K_{F,c}^2}{2m_c},$$
$$B_3 = \sum_{c=a,b} \frac{2K_{F,c}^5}{5\pi m_c^3}, \quad B_2 = \sum_{c=a,b} \frac{3K_{F,c}^4}{8m_c^3}. \quad (44)$$
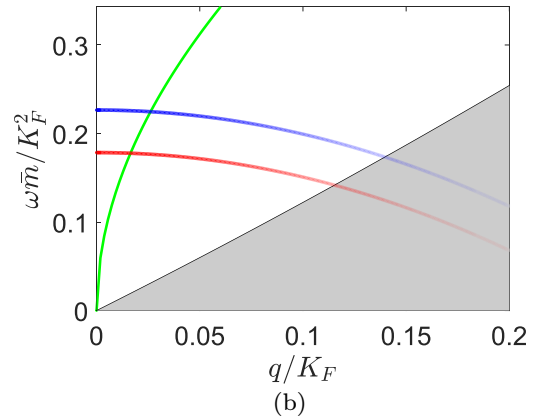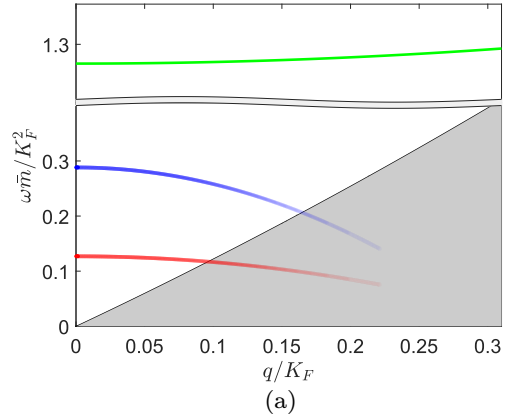

FIG. 9. Energy-momentum dispersions of the s-wave exciton and antiexciton bands (the red and blue lines), plasmon bands (the green lines), and continuum spectra of the intraband individual excitations (the grey shaded regions). The dispersions for $\bar{m} = m_a = m_b$ are determined by three dimensionless quantities, $K_F \alpha_B$, $\tilde{E}_g \equiv E_g \bar{m}/K_F^2$, and $\tilde{\mu} \equiv \mu \bar{m}/K_F^2$, where $K_F \equiv (K_{F,a} + K_{F,b})/2$ and the effective Bohr radius $\alpha_B \equiv 1/\bar{m}$. (a) The 3D case with $K_F \alpha_B = 0.289$, $\tilde{E}_g = -1.03$, and $\tilde{\mu} = 0.172$. (b) The 2D case with $K_F \alpha_B = 0.540$, $\tilde{E}_g = -1.03$, and $\tilde{\mu} = 0.172$. The quantum numbers of the s-wave exciton and antiexciton are $(nlm) = (100)$ in the 3D case and $(nm) = (10)$ in the 2D case (see the text).

Figure 9 shows the region of the continuum spectra of the intraband individual excitations, the dispersions of the plasmon modes, and momentum-energy dispersions of the s-wave exciton and antiexciton bands. The band dispersions for the exciton and antiexciton bands are calculated only around the Γ point [see Eqs. (A63) and Appendix A]. The figure shows that the plasmon oscillation in the 3D case appears at much higher energies than the exciton and antiexciton bands. Thereby, it is likely that the exciton-antiexciton pair in the 3D case only decays into (is only created from) intraband individual excitations. In the 2D case, the plasmon dispersion is gapless, where an exciton-antiexciton pair decays into (is created from) either interband individual excitations or density-wave modes.

VIII. SUMMARY

In this paper, we demonstrate the universal coexistence of the exciton and the antiparticle analog of the exciton (antiexciton) in semimetals as two distinguishable collective

modes. The concept of the antiparticle of exciton in semimetals is introduced by a spectral representation of the interband two-particle Green's function, and physical differences between our concept of the antiexciton and those in literature [17,18,20,21] are clarified. Evaluations of the Green's function in the dilute carrier-density limit show that the exciton and the antiexciton coexist in the interband excitation spectra of doped semimetals in two and three dimensions. The effective Lagrangian of the exciton and antiexciton is given by the *CP*-violated Klein-Gordon theory. The physical consequence of the coexistence of exciton and antiexciton is discussed in the optical spectroscopy experiment. Our theory is relevant to interband excitation spectra in semimetal materials, such as As, Sb, and HgTe, and electron-hole double-layer systems such as semiconductor heterostructures [33–40] and bilayer graphene under an external perpendicular electric field [41–43]. Optical absorption and photoluminescence can be experimental probes of the antiparticle analog of the exciton in these materials [44–47].

APPENDIX A: ENERGY BANDS OF THE EXCITON AND ANTIEXCITON AROUND THE Γ POINT

In this Appendix, we explain how we diagonalize Eq. (20) around $q = 0$ and obtain energy bands of the interband bound states around the Γ point. For clarity of presentation, we consider the case with $K_{F,a} > K_{F,b}$ ($\mu > \mu_0$). A generalization to the other case is straightforward.

For $|q|$ smaller than $K_{F,a} - K_{F,b}$ (including $q = 0$), the diagonal matrix $[\widetilde{G}_0^{ex}(q, \omega)^{-1}]_{kk'}$ has no finite matrix element for $K_{F,a} > |k + q|$ and $|k| > K_{F,b}$:

$$\widetilde{G}_0^{ex}(q, \omega)_{kk'}^{-1}$$
$$= \delta_{kk'} \begin{cases} \omega - [\epsilon_a(k + q) - \epsilon_b(k)], & |k + q| > K_{F,a} \\ -\{\omega - [\epsilon_a(k + q) - \epsilon_b(k)]\}, & |k| < K_{F,b}. \end{cases}$$
(A1)

Therefore, $[\widetilde{G}^{ex}(q, \omega)^{-1}]_{kk'}$ has finite matrix elements only within a domain of (i) $|k + q| > K_{F,a}$ or $K_{F,b} > |k|$ and (ii) $|k' + q| > K_{F,a}$ or $K_{F,b} > |k'|$:

$$\widetilde{G}^{ex}(q, \omega)^{-1} = \widetilde{G}_0^{ex}(q, \omega)^{-1} + \eta W \eta. \quad (A2)$$

Here η is a diagonal matrix,

$$[\eta]_{kk'} \equiv \delta_{kk'}[1 - \theta(K_{F,a} - |k + q|)\theta(|k| - K_{F,b})]. \quad (A3)$$

One can readily see this from a Taylor expansion of Eq. (20) in W for $\widetilde{G}^{ex}$:

$$\widetilde{G}^{ex} = \widetilde{G}_0^{ex} - \widetilde{G}_0^{ex} W \widetilde{G}_0^{ex} + \widetilde{G}_0^{ex} W \widetilde{G}_0^{ex} W \widetilde{G}_0^{ex} + \cdots, \quad (A4)$$

together with $\widetilde{G}_0^{ex} = \eta \widetilde{G}_0^{ex} \eta$. In the next two sections, we diagonalize $\widetilde{G}^{ex,-1}$ within the domain specified by Eq. (A3).

1. Interband excitation energies at the Γ point

When $q = 0$, $G^{ex}(0, \omega)^{-1}$ becomes real symmetric and it has continuous spatial rotation symmetries. Equation (21) can be block diagonalized in terms of spherical harmonics in three dimensions and trigonometric functions in two dimensions. This leads to Eq. (27) and Eq. (28). In this section, we will describe this deduction and how the radial functions in Eq. (27) and Eq. (28) should be calculated. With $\overline{G^{ex}}(q, \omega; k, k') \equiv \Omega \widetilde{G}^{ex}(q, \omega)_{kk'}$, the BS equation at $q = 0$ is given by

$$\int \frac{d^d k''}{(2\pi)^d} (D(\omega; k)(2\pi)^d \delta(k - k'') + w(k - k''))$$
$$\times \overline{G^{ex}}(0, \omega; k'', k') = (2\pi)^d \delta(k - k'), \quad (A5)$$

and

$$D(\omega; k) = \theta(|k| - K_{out})(\omega - (\epsilon_a(k) - \epsilon_b(k)))$$
$$- \theta(K_{in} - |k|)(\omega - (\epsilon_a(k) - \epsilon_b(k))). \quad (A6)$$

Note that k, k', and k'' in the equations are in a range $|k| > K_{F,a} \equiv K_{out}$ or $|k| < K_{F,b} \equiv K_{in}$. $\overline{G^{ex}}(q, \omega)_{kk'} = 0$ if k or k' is outside the range.

a. 3D case

In the 3D case, the δ function on the right-hand side of Eq. (A5) as well as the screened Coulomb interaction can be decomposed in terms of the spherical harmonics,

$$\delta(k - k') = \frac{1}{k^2} \delta(k - k') \delta(\cos\theta - \cos\theta') \delta(\varphi - \varphi')$$
$$= \frac{1}{k^2} \delta(k - k') \sum_{lm} Y_{lm}(\theta, \varphi) Y_{lm}^*(\theta', \varphi'), \quad (A7)$$

$$w(k - k') = \frac{4\pi}{k^2 + k'^2 - 2kk' \cos\gamma + k_{TF}^2}$$
$$= \sum_{lm} a_l(k, k') \frac{4\pi}{2l + 1} Y_{lm}(\theta, \varphi) Y_{lm}^*(\theta', \varphi'). \quad (A8)$$

Here $k \equiv (k \sin\theta \cos\varphi, k \sin\theta \sin\varphi, k \cos\theta)$. γ is an angle between k and k'. $P_l(\cos\gamma)$ is the Legendre polynomial ($l = 0, 1, \ldots$). $Y_{lm}(\theta, \varphi)$ is the spherical harmonics ($m = -l, -l + 1, \ldots, l$). The spherical harmonics are defined with normalization and completeness relations,

$$\int_{-1}^{1} d(\cos\theta) \int_0^{2\pi} d\varphi Y_{lm}^*(\theta, \varphi) Y_{l'm'}(\theta, \varphi) = \delta_{ll'} \delta_{mm'},$$
$$\sum_{lm} Y_{lm}(\theta, \varphi) Y_{lm}^*(\theta', \varphi') = \delta(\cos\theta - \cos\theta') \delta(\varphi - \varphi').$$
(A9)

$a_l(k, k')$ is the coefficient of the Legendre expansion. The lowest- and second-lowest-order coefficients are calculated as

$$a_0(k, k') = \frac{\pi}{kk'} \{ \ln((k + k')^2 + k_{TF}^2)$$
$$- \ln((k - k')^2 + k_{TF}^2) \}, \quad (A10)$$

$$a_1(k, k') = \frac{3\pi}{kk'} \left\{ \frac{k^2 + k'^2 + k_{TF}^2}{2kk'} \left[\ln\left((k + k')^2 + k_{TF}^2\right) \right. \right.$$
$$\left. \left. - \ln\left((k - k')^2 + k_{TF}^2\right) \right] - 2 \right\}. \quad (A11)$$

In terms of the harmonics, the solution of Eq. (A5) is given by

$$\overline{G^{ex}}(\mathbf{0}, \omega; \mathbf{k''}, \mathbf{k'})$$
$$= \sum_{nlm} \frac{Y_{lm}(\theta'', \varphi'') f_{nl}(\omega; k'') f_{nl}(\omega; k') Y_{lm}^*(\theta', \varphi')}{\xi_{nl}(\omega)}. \quad (A12)$$

Here $f_{nl}(\omega; k)$ and $\xi_{nl}(\omega)$ are the eigenvector and eigenvalue of a one-dimensional integral equation,

$$\int_0^\infty \frac{k'^2 dk'}{(2\pi)^3} h_l(\omega; k, k') f_{nl}(\omega; k') = \xi_{nl}(\omega) f_{nl}(\omega; k), \quad (A13)$$

with

$$h_l(\omega; k, k') \equiv \frac{D(\omega; k)}{k^2} (2\pi)^3 \delta(k - k') + \frac{4\pi}{2l+1} a_l(k, k'), \quad (A14)$$

and normalization and completeness relations,

$$\sum_n f_{nl}(\omega; k) f_{nl}(\omega; k') = \frac{(2\pi)^3}{k^2} \delta(k - k'),$$
$$\int_0^\infty \frac{k^2 dk}{(2\pi)^3} f_{nl}(\omega; k) f_{n'l}(\omega; k) = \delta_{nn'}. \quad (A15)$$

To solve the one-dimensional integral equation numerically, k is discretized by $2\pi/L$ with large L:

$$\int_0^\infty dk = \frac{2\pi}{L} \sum_k, \quad \delta(k - k') = \frac{L}{2\pi} \delta_{kk'}. \quad (A16)$$

With the discretization, the integral equation takes the form of

$$\sum_{k'} H_{l,kk'}^\omega V_{nl,k'}^\omega = \xi_{nl}(\omega) V_{nl,k}^\omega, \quad (A17)$$

and

$$H_{l,kk'}^\omega \equiv D(\omega; k) \delta_{kk'} + \frac{1}{L} \frac{kk'}{\pi} \frac{a_l(k, k')}{2l+1}, \quad (A18)$$
$$V_{nl,k}^\omega \equiv \frac{k}{2\pi\sqrt{L}} f_{nl}(\omega; k),$$

where $\sum_k V_{nl,k}^\omega V_{n'l,k}^\omega = \delta_{nn'}$ and $\sum_n V_{nl,k}^\omega V_{nl,k'}^\omega = \delta_{kk'}$.

b. 2D case

In the 2D case, the δ function and the screened Coulomb interaction are expanded in terms of the trigonometric

functions,

$$\delta(\mathbf{k} - \mathbf{k'}) = \frac{\delta(k - k')}{k} \delta(\varphi - \varphi')$$
$$= \frac{\delta(k - k')}{k} \frac{1}{2\pi} \sum_m e^{im(\varphi - \varphi')}, \quad (A19)$$

$$w(\mathbf{k} - \mathbf{k'}) = \frac{2\pi}{\sqrt{k^2 + k'^2 - 2kk' \cos(\varphi - \varphi')} + k_{TF}}$$
$$= \sum_m F_m(k, k') e^{im(\varphi - \varphi')}, \quad (A20)$$

where $\mathbf{k} \equiv (k \cos\varphi, k \sin\varphi)$, and

$$F_m(k, k') = \int_0^\pi d\phi \frac{2 \cos(m\phi)}{\sqrt{k^2 + k'^2 - 2kk' \cos\phi} + k_{TF}}. \quad (A21)$$

In terms of the expansion, the solution of Eq. (A5) is given by

$$\overline{G^{ex}}(\mathbf{0}, \omega; \mathbf{k''}, \mathbf{k'})$$
$$= \sum_{nm} \frac{f_{nm}(\omega; k'') f_{nm}(\omega; k') e^{im(\varphi'' - \varphi')}}{\xi_{nm}(\omega)}. \quad (A22)$$

Here $f_{nm}(\omega; k)$ and $\xi_{nm}(\omega)$ are the eigenvector and eigenvalue of a one-dimensional integral equation,

$$\int_0^{+\infty} \frac{k' dk'}{2\pi} h_m(\omega; k, k') f_{nm}(\omega; k') = \xi_{nm}(\omega) f_{nm}(\omega; k), \quad (A23)$$

with

$$h_m(\omega; k, k') = \frac{D(\omega; k)}{k} (2\pi) \delta(k - k') + F_m(k, k'), \quad (A24)$$

and normalization and completeness relation

$$\sum_n f_{nm}(\omega; k) f_{nm}(\omega; k') = \frac{2\pi}{k} \delta(k - k'),$$
$$\int_0^{+\infty} \frac{k dk}{2\pi} f_{nm}(\omega; k) f_{n'm'}(\omega, k) = \delta_{nn'}. \quad (A25)$$

With the same discretization as Eq. (A16), the integral equation reduces to

$$\sum_{k'} H_{m,kk'}^\omega V_{nm,k'}^\omega = \xi_{nm}(\omega) V_{nm,k}^\omega, \quad (A26)$$

and

$$H_{m,kk'}^\omega \equiv D(\omega; k) \delta_{kk'} + \frac{\sqrt{kk''}}{L} F_m(k, k'), \quad (A27)$$
$$V_{nm,k}^\omega \equiv \sqrt{\frac{k}{L}} f_{nm}(\omega; k),$$

where $\sum_k V_{nm,k}^\omega V_{n'm,k}^\omega = \delta_{nn'}$ and $\sum_n V_{nm,k}^\omega V_{nm,k'}^\omega = \delta_{kk'}$. $F_m(k, k')$ in Eq. (A21) is evaluated numerically.

In the numerical diagonalization of Eqs. (A17) and (A26), we set a large value of L ($\sim300 \times 2\pi$) and a large cutoff of k ($>15 \times \max(K_{F,a}, K_{F,b})$) so that the numerical solutions of the eigenvalues are convergent.
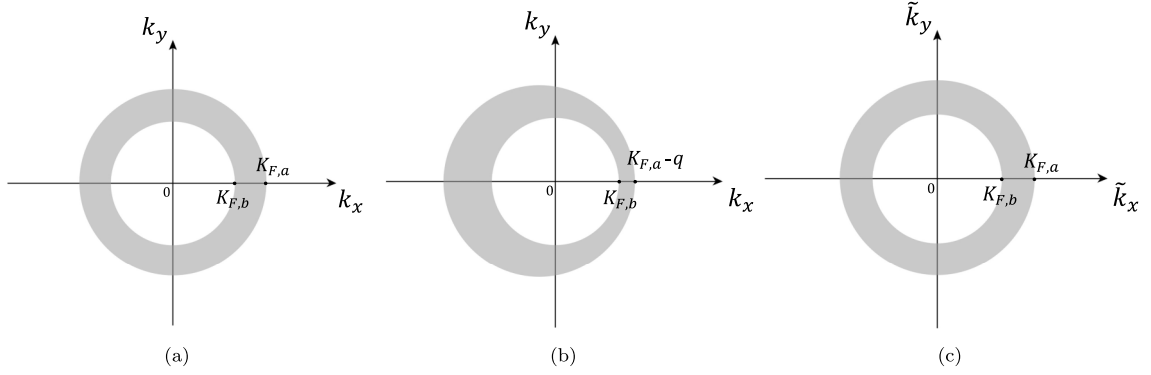
FIG. 10. Domains of $\widetilde{G}^{ex}(\mathbf{0}, \omega)^{-1}$ and $\widetilde{G}^{ex}(\mathbf{q}, \omega)^{-1}$. The shaded regions are excluded (a) for the domains of $\mathbf{k}$ and $\mathbf{k}'$ in $[\widetilde{G}^{ex}(\mathbf{0}, \omega)^{-1}]_{\mathbf{k}\mathbf{k}'}$, (b) for the domains of $\mathbf{k}$ and $\mathbf{k}'$ in $[\widetilde{G}^{ex}(\mathbf{q}, \omega)^{-1}]_{\mathbf{k}\mathbf{k}'}$, and (c) for the domains of $\tilde{\mathbf{k}}$ and $\tilde{\mathbf{k}}'$ in $[\widetilde{G}^{ex}(\mathbf{q}, \omega)^{-1}]_{\tilde{\mathbf{k}}\tilde{\mathbf{k}}'}$. We take $\mathbf{q} = q\mathbf{e}_x$ in the figure. The figures are plotted in the xy plane. For three dimensions, the y and z directions are symmetric.

2. Band curvatures of exciton and antiexciton bands around the Γ point

The previous section explains how we evaluate exciton and antiexciton energies at the Γ point. This section explains how we evaluate energy-band curvatures of the exciton and antiexciton bands around the Γ point. Let us begin with Eq. (21),

$$\sum_{\mathbf{k}'}[\widetilde{G}^{ex}(\mathbf{q}, \omega)^{-1}]_{\mathbf{k}\mathbf{k}'}\langle\mathbf{k}'|\phi_j(\mathbf{q}, \omega)\rangle = \xi_j(\mathbf{q}, \omega)\langle\mathbf{k}|\phi_j(\mathbf{q}, \omega)\rangle.$$

(A28)

$$\langle\mathbf{k}|\phi_j(\mathbf{q} = 0, \omega)\rangle = \begin{cases} \frac{1}{\sqrt{\Omega}}f_{nl}(\omega; k)Y_{lm}(\theta, \varphi), & j = (nlm), \text{ in three dimensions} \\ \frac{1}{\sqrt{\Omega}}f_{nm}(\omega; k)e^{im\varphi}, & j = (nm), \text{ in two dimensions.} \end{cases}$$

(A30)

The normalization gives a proper completeness relation,

$$\sum_j\langle\mathbf{k}|\phi_j(\mathbf{0}, \omega)\rangle\langle\phi_j(\mathbf{0}, \omega)|\mathbf{k}'\rangle = \delta_{\mathbf{k}\mathbf{k}'},$$

$$\sum_{\mathbf{k}}\langle\phi_j(\mathbf{0}, \omega)|\mathbf{k}\rangle\langle\mathbf{k}|\phi_{j'}(\mathbf{0}, \omega)\rangle = \delta_{jj'}.$$

(A31)

To obtain the band curvature of exciton and antiexciton bands around the Γ point, we consider $|\mathbf{q}|$ as a small quantity, expand $\widetilde{G}^{ex}(\mathbf{q}, \omega)^{-1}$ in $\mathbf{q}$ up to the second order, and evaluate the second-order energy correction of $\xi_j(\mathbf{q}, \omega)$: $\xi_j(\mathbf{q}, \omega) = \xi_j(\mathbf{0}, \omega) + b(\omega)q^2$. By the rotational symmetry, a q-linear energy correction is zero, while the q-quadratic energy correction depends only on the norm of $\mathbf{q}$, $q \equiv |\mathbf{q}|$.

Note that the domain of $\mathbf{k}$ and $\mathbf{k}'$ for $[\widetilde{G}^{ex}(\mathbf{0}, \omega)^{-1}]_{\mathbf{k}\mathbf{k}'}$ [Fig. 10(a)] and that for $[\widetilde{G}^{ex}(\mathbf{q}, \omega)^{-1}]_{\mathbf{k}\mathbf{k}'}$ [Fig. 10(b)] are different from each other. To rewrite this difference into a difference in the matrix elements, we adjust the domain of $[\widetilde{G}^{ex}(\mathbf{q}, \omega)^{-1}]$ into the domain of $[\widetilde{G}^{ex}(\mathbf{0}, \omega)^{-1}]$ by defining the following two new variables as replacements of $\mathbf{k}$ and $\mathbf{k}'$, respectively:

$$\tilde{\mathbf{k}} \equiv \begin{cases} \mathbf{k} + \mathbf{q}, & |\mathbf{k} + \mathbf{q}| > K_{F,a} \\ \mathbf{k}, & |\mathbf{k}| < K_{F,b}, \end{cases}$$

Suppose that the eigenvalue problem at $\mathbf{q} = 0$ is solved for the 3D and 2D cases, respectively, as in the previous section:

$$\sum_{\mathbf{k}'}[\widetilde{G}^{ex}(\mathbf{0}, \omega)^{-1}]_{\mathbf{k}\mathbf{k}'}\langle\mathbf{k}'|\phi_j(\mathbf{0}, \omega)\rangle = \xi_j(\mathbf{0}, \omega)\langle\mathbf{k}|\phi_j(\mathbf{0}, \omega)\rangle,$$

(A29)

with a normalization,

$$\tilde{\mathbf{k}}' \equiv \begin{cases} \mathbf{k}' + \mathbf{q}, & |\mathbf{k}' + \mathbf{q}| > K_{F,a} \\ \mathbf{k}', & |\mathbf{k}'| < K_{F,b}. \end{cases}$$

(A32)

In terms of the new variables, $[\widetilde{G}^{ex}(\mathbf{q}, \omega)^{-1}]_{\tilde{\mathbf{k}}\tilde{\mathbf{k}}'}$ shares the identical domain [Fig. 10(c)] with $[\widetilde{G}^{ex}(0, \omega)^{-1}]_{\tilde{\mathbf{k}}\tilde{\mathbf{k}}'}$: (i) $|\tilde{\mathbf{k}}| > K_{F,a}$ or $K_{F,b} > |\tilde{\mathbf{k}}|$ and (ii) $|\tilde{\mathbf{k}}'| > K_{F,a}$ or $K_{F,b} > |\tilde{\mathbf{k}}'|$. Let us compare their matrix elements in the domain. In terms of the new variables, $\widetilde{G}^{ex,-1} = \widetilde{G}_0^{ex,-1} + W$ is given by

$$\left[\widetilde{G}_0^{ex,-1}(\mathbf{q}, \omega)\right]_{\tilde{\mathbf{k}}\tilde{\mathbf{k}}'}$$

$$= \delta_{\tilde{\mathbf{k}}\tilde{\mathbf{k}}'}\begin{cases} \omega - [\epsilon_a(\tilde{\mathbf{k}}) - \epsilon_b(\tilde{\mathbf{k}} - \mathbf{q})], & |\tilde{\mathbf{k}}| > K_{F,a} \\ -\{\omega - [\epsilon_a(\tilde{\mathbf{k}} + \mathbf{q}) - \epsilon_b(\tilde{\mathbf{k}})]\}, & |\tilde{\mathbf{k}}| < K_{F,b}, \end{cases}$$

(A33)

$$[W]_{\tilde{\mathbf{k}}\tilde{\mathbf{k}}'} = \begin{cases} \frac{w(\tilde{\mathbf{k}} - \tilde{\mathbf{k}}')}{\Omega} & |\tilde{\mathbf{k}}| > K_{F,a}, \ |\tilde{\mathbf{k}}'| > K_{F,a} \\ \frac{w(\tilde{\mathbf{k}} - \tilde{\mathbf{k}}')}{\Omega} & |\tilde{\mathbf{k}}| < K_{F,b}, \ |\tilde{\mathbf{k}}'| < K_{F,b} \\ \frac{w(\tilde{\mathbf{k}} - \mathbf{q} - \tilde{\mathbf{k}}')}{\Omega} & |\tilde{\mathbf{k}}| > K_{F,a}, \ |\tilde{\mathbf{k}}'| < K_{F,b} \\ \frac{w(\tilde{\mathbf{k}} - \tilde{\mathbf{k}}' + \mathbf{q})}{\Omega} & |\tilde{\mathbf{k}}| < K_{F,b}, \ |\tilde{\mathbf{k}}'| > K_{F,a}. \end{cases}$$

(A34)

In the following, we take $\mathbf{q} = q\mathbf{e}_i$ ($\mathbf{e}_i$ is a unit vector along i, $i = x, y, z$) and take q derivatives of the $\widetilde{G}^{ex}(\mathbf{q}, \omega)_{\tilde{\mathbf{k}}\tilde{\mathbf{k}}'}^{-1}$ matrix around the $\mathbf{q} = 0$ point.

For simplicity of the presentation, let us call the new variables $\tilde{\mathbf{k}}$ and $\tilde{\mathbf{k}}'$ as $\mathbf{k}$ and $\mathbf{k}'$. The first q derivative of $\widetilde{G}^{ex}(\mathbf{q}, \omega)_{\mathbf{k}\mathbf{k}'}^{-1}$

is given by

$$
[\boldsymbol{F}_i]_{\boldsymbol{k}\boldsymbol{k}'} \equiv \left[\frac{\partial \widetilde{G}^{ex}(q\boldsymbol{e}_i, \omega)^{-1}}{\partial q} \Big|_{q=0} \right]_{\boldsymbol{k}\boldsymbol{k}'} = \begin{cases} \frac{k_i}{m_b} & |\boldsymbol{k}| > K_{F,a}, \quad \boldsymbol{k} = \boldsymbol{k}' \\ \frac{k_i}{m_a} & |\boldsymbol{k}| < K_{F,b}, \quad \boldsymbol{k} = \boldsymbol{k}' \\ 0 & |\boldsymbol{k}| < K_{F,b}, \quad |\boldsymbol{k}'| < K_{F,b}, \quad \boldsymbol{k} \neq \boldsymbol{k}' \\ 0 & |\boldsymbol{k}| > K_{F,a}, \quad |\boldsymbol{k}'| > K_{F,a}, \quad \boldsymbol{k} \neq \boldsymbol{k}' \\ \frac{1}{\Omega} \frac{\partial w(\boldsymbol{k}-\boldsymbol{k}'+q\boldsymbol{e}_i)}{\partial q}|_{q=0} & |\boldsymbol{k}| < K_{F,b}, \quad |\boldsymbol{k}'| > K_{F,a} \\ \frac{1}{\Omega} \frac{\partial w(\boldsymbol{k}-q\boldsymbol{e}_i-\boldsymbol{k}')}{\partial q}|_{q=0} & |\boldsymbol{k}| > K_{F,a}, \quad |\boldsymbol{k}'| < K_{F,b}, \end{cases}
\tag{A35}
$$

with

$$
\frac{\partial w(\boldsymbol{k} - \boldsymbol{k}' + q\boldsymbol{e}_i)}{\partial q}\Big|_{q=0} = \begin{cases} -\frac{4\pi \times 2(k_i - k_i')}{(|\boldsymbol{k}-\boldsymbol{k}'|^2 + k_{TF}^2)^2} & \text{in three dimensions} \\ -\frac{2\pi}{(|\boldsymbol{k}-\boldsymbol{k}'| + k_{TF})^2} \frac{k_i - k_i'}{|\boldsymbol{k}-\boldsymbol{k}'|} & \text{in two dimensions.} \end{cases}
\tag{A36}
$$

The second q derivative of $\widetilde{G}^{ex}(\boldsymbol{q}, \omega)_{\boldsymbol{k}\boldsymbol{k}'}^{-1}$ is given by

$$
2[\boldsymbol{S}_i]_{\boldsymbol{k}\boldsymbol{k}'} \equiv \left[\frac{\partial^2 \widetilde{G}^{ex}(q\boldsymbol{e}_i, \omega)^{-1}}{\partial q^2} \Big|_{q=0} \right]_{\boldsymbol{k}\boldsymbol{k}'} = \begin{cases} -\frac{1}{m_b} & |\boldsymbol{k}| > K_{F,a}, \quad \boldsymbol{k} = \boldsymbol{k}' \\ \frac{1}{m_a} & |\boldsymbol{k}| < K_{F,b}, \quad \boldsymbol{k} = \boldsymbol{k}' \\ 0 & |\boldsymbol{k}| < K_{F,b}, \quad |\boldsymbol{k}'| < K_{F,b}, \quad \boldsymbol{k} \neq \boldsymbol{k}' \\ 0 & |\boldsymbol{k}| > K_{F,a}, \quad |\boldsymbol{k}'| > K_{F,a}, \quad \boldsymbol{k} \neq \boldsymbol{k}' \\ \frac{1}{\Omega} \frac{\partial^2 w(\boldsymbol{k}-\boldsymbol{k}'+q\boldsymbol{e}_i)}{\partial q^2}|_{q=0} & |\boldsymbol{k}| < K_{F,b}, \quad |\boldsymbol{k}'| > K_{F,a} \\ \frac{1}{\Omega} \frac{\partial^2 w(\boldsymbol{k}-q\boldsymbol{e}_i-\boldsymbol{k}')}{\partial q^2}|_{q=0} & |\boldsymbol{k}| > K_{F,a}, \quad |\boldsymbol{k}'| < K_{F,b}, \end{cases}
\tag{A37}
$$

with

$$
\frac{\partial^2 w(\boldsymbol{k} - \boldsymbol{k}' + q\boldsymbol{e}_i)}{\partial q^2}\Big|_{q=0} = -\frac{8\pi}{\left(|\boldsymbol{k}-\boldsymbol{k}'|^2 + k_{TF}^2\right)^2} + \frac{32\pi (k_i - k_i')^2}{\left(|\boldsymbol{k}-\boldsymbol{k}'|^2 + k_{TF}^2\right)^3}
\tag{A38}
$$

in three dimensions and

$$
\frac{\partial^2 w(\boldsymbol{k} - \boldsymbol{k}' + q\boldsymbol{e}_i)}{\partial q^2}\Big|_{q=0} = -\frac{2\pi}{(|\boldsymbol{k}-\boldsymbol{k}'| + k_{TF})^2} \frac{1}{|\boldsymbol{k}-\boldsymbol{k}'|} + \frac{4\pi}{(|\boldsymbol{k}-\boldsymbol{k}'| + k_{TF})^3} \frac{(k_i - k_i')^2}{|\boldsymbol{k}-\boldsymbol{k}'|^2} + \frac{2\pi}{(|\boldsymbol{k}-\boldsymbol{k}'| + k_{TF})^2} \frac{(k_i - k_i')^2}{|\boldsymbol{k}-\boldsymbol{k}'|^3}
\tag{A39}
$$

in two dimensions. Now that $\widetilde{G}^{ex}(q\boldsymbol{e}_i, \omega)^{-1}$ is expanded in q,

$$
[\widetilde{G}^{ex}(q\boldsymbol{e}_i, \omega)^{-1}] = [\widetilde{G}^{ex}(\boldsymbol{0}, \omega)^{-1}] + [\boldsymbol{F}_i]q + [\boldsymbol{S}_i]q^2 + \mathcal{O}(q^3),
\tag{A40}
$$

the second-order perturbation theory gives the second-order energy correction,

$$
\xi_j(q\boldsymbol{e}_i, \omega) = \xi_j(\boldsymbol{0}, \omega) + b_j(\omega)q^2 + \mathcal{O}(q^3).
\tag{A41}
$$

Here $b_j(\omega)$ is given by the eigenvectors and eigenvalues at $\boldsymbol{q} = 0$ [see Eqs. (A29) and (A30)],

$$
b_j(\omega) = \sum_{j' \neq j} \frac{\langle \phi_j(\boldsymbol{0}, \omega)|\boldsymbol{F}_i|\phi_{j'}(\boldsymbol{0}, \omega)\rangle \langle \phi_{j'}(\boldsymbol{0}, \omega)|\boldsymbol{F}_i|\phi_j(\boldsymbol{0}, \omega)\rangle}{\xi_j(\boldsymbol{0}, \omega) - \xi_{j'}(\boldsymbol{0}, \omega)} + \langle \phi_j(\boldsymbol{0}, \omega)|\boldsymbol{S}_i|\phi_j(\boldsymbol{0}, \omega)\rangle \equiv F_2 + S_1.
\tag{A42}
$$

The previous section describes how to calculate the eigenvectors and eigenvalues of the lowest-energy s-wave exciton and antiexciton at $\boldsymbol{q} = 0$ in the 3D case [$j \equiv (nlm) = (100)$] and 2D case [$j = (nm) = (10)$]. In the following, we will describe how to calculate $b_{(100)}(\omega = \pm\omega_\pm)$ in the 3D case and $b_{(10)}(\omega = \pm\omega_\pm)$ in the 2D case.

a. 3D case

Consider the 3D case with $j \equiv (nlm)$ and take $(nlm) = (100)$ and $\boldsymbol{e}_i = \boldsymbol{e}_z$. Since $\xi_j(\boldsymbol{q} = \boldsymbol{0}, \omega = \pm\omega_\pm) = 0$, F_2 is given by

$$
F_2 = -\sum_{nlm \neq (100)} \sum_{\boldsymbol{k}_1, \boldsymbol{k}_2, \boldsymbol{k}_3, \boldsymbol{k}_4} \xi_{nl}^{-1}(\boldsymbol{0}, \omega) \langle \phi_{100}(\boldsymbol{0}, \omega)|\boldsymbol{k}_1\rangle [\boldsymbol{F}_z]_{\boldsymbol{k}_1 \boldsymbol{k}_2} \langle \boldsymbol{k}_2|\phi_{nlm}(\boldsymbol{0}, \omega)\rangle \langle \phi_{nlm}(\boldsymbol{0}, \omega)|\boldsymbol{k}_3\rangle [\boldsymbol{F}_z]_{\boldsymbol{k}_3 \boldsymbol{k}_4} \langle \boldsymbol{k}_4|\phi_{100}(\boldsymbol{0}, \omega)\rangle,
\tag{A43}
$$

at $\omega = \pm\omega_{\pm}$. In terms of Eq. (A30) and $Y_{00}(\theta, \varphi) = \frac{1}{2\sqrt{\pi}}$, we evaluate matrix elements of $\boldsymbol{F}_z$ by three-dimensional momentum integrals:

$$
\sum_{\boldsymbol{k}_1, \boldsymbol{k}_2} \langle \phi_{100}(\boldsymbol{0}, \omega) | \boldsymbol{k}_1 \rangle [\boldsymbol{F}_z]_{\boldsymbol{k}_1 \boldsymbol{k}_2} \langle \boldsymbol{k}_2 | \phi_{nlm}(\boldsymbol{0}, \omega) \rangle
$$

$$
= \left(\prod_{i=1}^{2} \int_0^{+\infty} \frac{dk_i}{(2\pi)^3} \; k_i^2 \int_{-1}^{1} d\cos\theta_i \int_0^{2\pi} d\varphi_i \right) f_{10}(\omega; k_1) \frac{1}{2\sqrt{\pi}} \Omega[\boldsymbol{F}_z]_{\boldsymbol{k}_1 \boldsymbol{k}_2} f_{nl}(\omega; k_2) Y_{lm}(\theta_2, \varphi_2), \tag{A44}
$$

with

$$
\Omega[\boldsymbol{F}_z]_{\boldsymbol{k}_1 \boldsymbol{k}_2} = \left(\theta(k_1 - K_{F,a}) \frac{k_1 \cos\theta_1}{m_b} + \theta(K_{F,b} - k_1) \frac{k_1 \cos\theta_1}{m_a} \right) \frac{(2\pi)^3}{k_1^2} \delta(k_1 - k_2) \sum_{lm} Y_{lm}(\theta_1, \varphi_1) Y_{lm}^*(\theta_2, \varphi_2)
$$

$$
+ 2 \sum_{lm} b_l(k_1, k_2) \frac{4\pi}{2l+1} Y_{lm}(\theta_1, \varphi_1) Y_{lm}^*(\theta_2, \varphi_2) (\theta(k_1 - K_{F,a})\theta(K_{F,b} - k_2)(k_1 \cos\theta_1 - k_2 \cos\theta_2)
$$

$$
+ \theta(k_2 - K_{F,a})\theta(K_{F,b} - k_1)(k_2 \cos\theta_2 - k_1 \cos\theta_1)). \tag{A45}
$$

Here $\boldsymbol{k}_j \equiv k_j(\sin\theta_j \cos\varphi_j, \sin\theta_j \sin\varphi_j, \cos\theta_j)$ $(j = 1, 2, 3, 4)$. We used the spherical expansion of Eq. (A36):

$$
\frac{4\pi}{(|\boldsymbol{k}_1 - \boldsymbol{k}_2|^2 + k_{TF}^2)^2} = \sum_l b_l(k_1, k_2) P_l(\cos\gamma) = \sum_{lm} b_l(k_1, k_2) \frac{4\pi}{2l+1} Y_{lm}(\theta_1, \varphi_1) Y_{lm}^*(\theta_2, \varphi_2). \tag{A46}
$$

The lowest- and second-lowest expansion coefficients are calculated as

$$
b_0(k_1, k_2) = \frac{\pi}{k_1 k_2} \left(\frac{1}{(k_1 - k_2)^2 + k_{TF}^2} - \frac{1}{(k_1 + k_2)^2 + k_{TF}^2} \right), \tag{A47}
$$

$$
b_1(k_1, k_2) = \frac{3\pi}{2(k_1 k_2)^2} \left\{ \ln \left[\frac{(k_1 - k_2)^2 + k_{TF}^2}{(k_1 + k_2)^2 + k_{TF}^2} \right] + (k_1^2 + k_2^2 + k_{TF}^2) \left[\frac{1}{(k_1 - k_2)^2 + k_{TF}^2} - \frac{1}{(k_1 + k_2)^2 + k_{TF}^2} \right] \right\}. \tag{A48}
$$

After the momentum integrals in Eq. (A44), only the $(lm) = (10)$ term remains finite in Eq. (A44). With $\cos\theta = 2\sqrt{\frac{\pi}{3}} Y_{10}^*(\theta, \varphi)$, the nonzero term is evaluated as

$$
\langle \phi_{100}(\boldsymbol{0}, \omega) | \boldsymbol{F}_z | \phi_{nlm}(\boldsymbol{0}, \omega) \rangle = \delta_{l1}\delta_{m0} \frac{4}{\sqrt{3}} \left(\prod_{i=1}^{2} \int_0^{+\infty} \frac{dk_i}{(2\pi)^3} \; k_i^2 \right) f_{10}(\omega; k_1) \rho(k_1, k_2) f_{n1}(\omega; k_2), \tag{A49}
$$

with

$$
\rho(k_1, k_2) = \left(\frac{\theta(k_1 - K_{F,a})}{m_b} + \frac{\theta(K_{F,b} - k_1)}{m_a} \right) (2\pi)^3 \frac{\delta(k_1 - k_2)}{k_1} + 8\pi \left(\theta(k_1 - K_{F,a})\theta(K_{F,b} - k_2) \right.
$$

$$
\times \left(\frac{1}{3} b_1(k_1, k_2) k_1 - b_0(k_1, k_2) k_2 \right) + \theta(k_2 - K_{F,a})\theta(K_{F,b} - k_1)(b_0(k_1, k_2) k_2 - \frac{1}{3} b_1(k_1, k_2) k_1) \right). \tag{A50}
$$

Then we finally have

$$
F_2 = -\frac{1}{3} \left(\prod_{i=1}^{4} \int_0^{+\infty} \frac{dk_i}{(2\pi)^3} \; k_i^2 \right) \sum_n \frac{1}{\xi_{n1}(\boldsymbol{0}, \omega)} f_{10}(\omega; k_1) \rho(k_1, k_2) f_{n1}(\omega; k_2) f_{n1}(\omega; k_3) \rho(k_3, k_4) f_{10}(\omega; k_4). \tag{A51}
$$

To numerically evaluate Eq. (A51), we use the same discretization of k as in Eq. (A16),

$$
F_2 = -\frac{1}{3} \sum_{k_1, k_2, k_3, k_4, n} \frac{V_{10, k_1}^{\omega} P_{k_1 k_2} V_{n1, k_2}^{\omega} V_{n1, k_3}^{\omega} P_{k_3 k_4} V_{10, k_4}^{\omega}}{\xi_{n1}(\boldsymbol{0}, \omega)} = -\frac{1}{3} \sum_{k_1, k_2, k_3, k_4} V_{10, k_1}^{\omega} P_{k_1 k_2} H_{1, k_2 k_3}^{\omega, -1} P_{k_3 k_4} V_{10, k_4}^{\omega}. \tag{A52}
$$

$V_{nl, k}^{\omega}$ and $H_{1, kk'}^{\omega}$ are defined in Eq. (A18) and

$$
P_{k_1 k_2} = \frac{k_1 k_2}{L(2\pi)^2} \rho(k_1, k_2) = \left(\theta(k_1 - K_{F,a}) \frac{k_1}{m_b} + \theta(K_{F,b} - k_1) \frac{k_1}{m_a} \right) \delta_{k_1 k_2} + \frac{8\pi k_1 k_2}{L(2\pi)^2} \left(\theta(k_1 - K_{F,a})\theta(K_{F,b} - k_2) \right.
$$

$$
\times \left(\frac{1}{3} b_1(k_1, k_2) k_1 - b_0(k_1, k_2) k_2 \right) + \theta(k_2 - K_{F,a})\theta(K_{F,b} - k_1)(b_0(k_1, k_2) k_2 - \frac{1}{3} b_1(k_1, k_2) k_1) \right). \tag{A53}
$$

S_1 in Eq. (A42) is given by

$$S_1 = \sum_{\boldsymbol{k}_1, \boldsymbol{k}_2} \langle \phi_{100}(\boldsymbol{0}, \omega) | \boldsymbol{k}_1 \rangle [S_z]_{\boldsymbol{k}_1 \boldsymbol{k}_2} \langle \boldsymbol{k}_2 | \phi_{100}(\boldsymbol{0}, \omega) \rangle = \frac{1}{3} \sum_{\boldsymbol{k}_1, \boldsymbol{k}_2} \langle \phi_{100}(\boldsymbol{0}, \omega) | \boldsymbol{k}_1 \rangle [S_z + S_x + S_y]_{\boldsymbol{k}_1 \boldsymbol{k}_2} \langle \boldsymbol{k}_2 | \phi_{100}(\boldsymbol{0}, \omega) \rangle$$

$$= \left(\prod_{i=1}^{2} \int_0^{+\infty} \frac{dk_i}{(2\pi)^3} \; k_i^2 \int_{-1}^{1} d\cos\theta_i \int_0^{2\pi} d\varphi_i \right) \frac{1}{4\pi} f_{10}(\omega; k_1) \Omega S(\boldsymbol{k}_1, \boldsymbol{k}_2) f_{10}(\omega; k_2), \tag{A54}$$

with

$$\Omega S(\boldsymbol{k}_1, \boldsymbol{k}_2) = \left(-\frac{\theta(k_1 - K_{F,a})}{2m_b} + \frac{\theta(K_{F,b} - k_1)}{2m_a} \right) \frac{(2\pi)^3}{k_1^2} \delta(k_1 - k_2) \sum_{lm} Y_{lm}(\theta_1, \varphi_1) Y_{lm}^*(\theta_2, \varphi_2)$$

$$+ \sum_{lm} \beta_l(k_1, k_2) \frac{4\pi}{2l+1} Y_{lm}(\theta_1, \varphi_1) Y_{lm}^*(\theta_2, \varphi_2) (\theta(k_1 - K_{F,a})\theta(K_{F,b} - k_2) + \theta(k_2 - K_{F,a})\theta(K_{F,b} - k_1)). \tag{A55}$$

Here we used the spherical expansion of Eq. (A38):

$$-\frac{4\pi}{(|\boldsymbol{k}_1 - \boldsymbol{k}_2|^2 + k_{TF}^2)^2} + \frac{4\pi \times 4|\boldsymbol{k}_1 - \boldsymbol{k}_2|^2/3}{(|\boldsymbol{k}_1 - \boldsymbol{k}_2|^2 + k_{TF}^2)^3} = \sum_{lm} \beta_l(k_1, k_2) \frac{4\pi}{2l+1} Y_{lm}(\theta_1, \varphi_1) Y_{lm}^*(\theta_2, \varphi_2). \tag{A56}$$

The lowest-order expansion coefficient is calculated as

$$\beta_0(k_1, k_2) = \frac{\pi}{3k_1 k_2} \left(\frac{1}{(k_1 - k_2)^2 + k_{TF}^2} - \frac{1}{(k_1 + k_2)^2 + k_{TF}^2} \right) - \frac{2\pi k_{TF}^2}{3k_1 k_2} \left(\frac{1}{((k_1 - k_2)^2 + k_{TF}^2)^2} - \frac{1}{((k_1 + k_2)^2 + k_{TF}^2)^2} \right). \tag{A57}$$

After the integration in Eq. (A54), only the $(lm) = (00)$ term in Eq. (A55) remains finite:

$$S_1 = \left(\prod_{i=1}^{2} \int_0^{+\infty} \frac{dk_i}{(2\pi)^3} \; k_i^2 \right) f_{10}(\omega; k_1) c(k_1, k_2) f_{10}(\omega; k_2), \tag{A58}$$

with

$$c(k_1, k_2) = \left(-\frac{\theta(k_1 - K_{F,a})}{2m_b} + \frac{\theta(K_{F,b} - k_1)}{2m_a} \right) (2\pi)^3 \frac{\delta(k_1 - k_2)}{k_1^2} + \beta_0(k_1, k_2)(4\pi)(\theta(k_1 - K_{F,a})\theta(K_{F,b} - k_2)$$

$$+ \theta(k_2 - K_{F,a})\theta(K_{F,b} - k_1)). \tag{A59}$$

To numerically evaluate Eq. (A58), we discretize k_1 and k_2 as in Eq. (A16),

$$S_1 = \sum_{k_1, k_2} V_{10,k_1}^{\omega} C_{k_1 k_2} V_{10,k_2}^{\omega}, \tag{A60}$$

with

$$C_{k_1 k_2} \equiv \frac{k_1 k_2}{L(2\pi)^2} c(k_1, k_2) = \left(-\frac{\theta(k_1 - K_{F,a})}{2m_b} + \frac{\theta(K_{F,b} - k_1)}{2m_a} \right) \delta_{k_1 k_2}$$

$$+ \frac{k_1 k_2}{L(2\pi)^2} \beta_0(k_1, k_2)(4\pi)(\theta(k_1 - K_{F,a})\theta(K_{F,b} - k_2) + \theta(k_2 - K_{F,a})\theta(K_{F,b} - k_1)). \tag{A61}$$

In summary, $b_j(\omega)$ is given by Eqs. (A42), (A52), and (A60) at $\omega = \pm\omega_\pm$. The energy-band curvatures of the lowest s-wave [$j = (100)$] exciton and antiexciton bands at the Γ point can be determined by $b_j(+\omega_+)$ and $b_j(-\omega_-)$, respectively:

$$\begin{cases} \xi_j(\boldsymbol{q}, \omega_+(\boldsymbol{q})) = (\omega_+(\boldsymbol{q}) - \omega_+) \big[\frac{d\xi_j(\boldsymbol{0}, \omega)}{d\omega} \big]_{|\omega = \omega_+} + b_j(\omega_+) q^2 = 0 & \text{for exciton} \\ \xi_j(\boldsymbol{q}, -\omega_-(\boldsymbol{q})) = (-\omega_-(\boldsymbol{q}) + \omega_-) \big[\frac{d\xi_j(\boldsymbol{0}, \omega)}{d\omega} \big]_{|\omega = -\omega_-} + b_j(-\omega_-) q^2 = 0 & \text{for antiexciton.} \end{cases} \tag{A62}$$

From this, we obtain the energy-band curvatures of the exciton and antiexciton around the Γ point,

$$\begin{cases} \omega_+(\boldsymbol{q}) = \omega_+ - b_j(\omega_+) \big[\frac{d\xi_j(\boldsymbol{0}, \omega)}{d\omega} \big]_{|\omega = \omega_+}^{-1} q^2 + \cdots & \text{for exciton} \\ \omega_-(\boldsymbol{q}) = \omega_- + b_j(-\omega_-) \big[\frac{d\xi_j(\boldsymbol{0}, \omega)}{d\omega} \big]_{|\omega = -\omega_-}^{-1} q^2 + \cdots & \text{for antiexciton.} \end{cases} \tag{A63}$$

b. 2D case

Consider the 2D case with $j = (nm)$ and take $(nm) = (10)$ and $\boldsymbol{e}_i = \boldsymbol{e}_x$. Since $\xi_j(\boldsymbol{0}, \pm \omega_\pm) = 0$, F_2 in Eq. (A42) is given by

$$F_2 = - \sum_{nm \neq 10} \sum_{\boldsymbol{k}_1, \boldsymbol{k}_2, \boldsymbol{k}_3, \boldsymbol{k}_4} \xi_{nm}^{-1}(\boldsymbol{0}, \omega) \langle \phi_{10}(\boldsymbol{0}, \omega) | \boldsymbol{k}_1 \rangle [\boldsymbol{F}_x]_{\boldsymbol{k}_1 \boldsymbol{k}_2} \langle \boldsymbol{k}_2 | \phi_{nm}(\boldsymbol{0}, \omega) \rangle \langle \phi_{nm}(\boldsymbol{0}, \omega) | \boldsymbol{k}_3 \rangle [\boldsymbol{F}_x]_{\boldsymbol{k}_3 \boldsymbol{k}_4} \langle \boldsymbol{k}_4 | \phi_{10}(\boldsymbol{0}, \omega) \rangle. \tag{A64}$$

In terms of Eq. (A30), we evaluate the matrix elements in F_2 by the 2D momentum integrals:

$$\sum_{\boldsymbol{k}_1, \boldsymbol{k}_2} \langle \phi_{10}(\boldsymbol{0}, \omega) | \boldsymbol{k}_1 \rangle [\boldsymbol{F}_x]_{\boldsymbol{k}_1 \boldsymbol{k}_2} \langle \boldsymbol{k}_2 | \phi_{nm}(\boldsymbol{0}, \omega) \rangle = \left(\prod_{i=1}^{2} \int_0^{+\infty} \frac{k_i dk_i}{2\pi} \int_0^{2\pi} \frac{d\varphi_i}{2\pi} \right) f_{10}(\omega; k_1) \Omega \boldsymbol{F}_x(\boldsymbol{k_1}, \boldsymbol{k_2}) f_{nm}(\omega; k_2) e^{im\varphi_2}. \tag{A65}$$

Equation (A36) is decomposed in terms of the trigonometric functions,

$$\frac{2\pi}{(|\boldsymbol{k_1} - \boldsymbol{k_2}| + k_{TF})^2} \frac{1}{|\boldsymbol{k_1} - \boldsymbol{k_2}|} = \sum_m J_m(k_1, k_2) e^{im(\varphi_1 - \varphi_2)},$$

with

$$J_m(k_1, k_2) = \int_0^{2\pi} \frac{d(\varphi_1 - \varphi_2)}{2\pi} e^{-im(\varphi_1 - \varphi_2)} \frac{2\pi}{\left(\sqrt{k_1^2 + k_2^2 - 2k_1 k_2 \cos(\varphi_1 - \varphi_2)} + k_{TF} \right)^2} \frac{1}{\sqrt{k_1^2 + k_2^2 - 2k_1 k_2 \cos(\varphi_1 - \varphi_2)}}. \tag{A66}$$

Equation (A64) is calculated in terms of the expansion,

$$\langle \phi_{10}(\boldsymbol{0}, \omega) | \boldsymbol{F}_x | \phi_{nm}(\boldsymbol{0}, \omega) \rangle$$

$$= \left(\prod_{i=1}^{2} \int_0^{+\infty} \frac{dk_i}{2\pi} k_i \int_0^{2\pi} \frac{d\varphi_i}{2\pi} \right) f_{10}(\omega; k_1) f_{nm}(\omega; k_2) e^{im\varphi_2} \left\{ \left(\frac{\theta(k_1 - K_{F,a})}{m_b} + \frac{\theta(K_{F,b} - k_1)}{m_a} \right) \right.$$

$$\times \pi \delta(k_1 - k_2)(e^{i\varphi_1} + e^{-i\varphi_1}) \sum_{m'} e^{im'(\varphi_1 - \varphi_2)} + \theta(k_1 - K_{F,a})\theta(K_{F,b} - k_2) \left(\frac{k_1(e^{i\varphi_1} + e^{-i\varphi_1})}{2} \right.$$

$$\left. - \frac{k_2(e^{i\varphi_2} + e^{-i\varphi_2})}{2} \right) \sum_{m'} J_{m'}(k_1, k_2) e^{im'\varphi_1} e^{-im'\varphi_2} + \theta(k_2 - K_{F,a})\theta(K_{F,b} - k_1) \left(\frac{k_2(e^{i\varphi_2} + e^{-i\varphi_2})}{2} \right.$$

$$\left. \left. - \frac{k_1(e^{i\varphi_1} + e^{-i\varphi_1})}{2} \right) \sum_{m'} J_{m'}(k_1, k_2) e^{im'\varphi_1} e^{-im'\varphi_2} \right\}. \tag{A67}$$

After the momentum integration in Eq. (A65), only $m = \pm 1$ terms remain finite in Eq. (A65). Since $f_{nm}(\omega; k) = f_{n(-m)}(\omega; k)$, $\xi_{nm}(\omega; k) = \xi_{n(-m)}(\omega; k)$, and $J_m(k, k') = J_{-m}(k, k')$, the matrix elements for $m = +1$ and those for $m = -1$ are the same,

$$\langle \phi_{10}(\boldsymbol{0}, \omega) | \boldsymbol{F}_x | \phi_{n(\pm 1)}(\boldsymbol{0}, \omega) \rangle = \left(\prod_{i=1}^{2} \int_0^{+\infty} \frac{dk_i}{2\pi} k_i \right) f_{10}(\omega; k_1) \tau(k_1, k_2) f_{n1}(\omega; k_2), \tag{A68}$$

with

$$\tau(k_1, k_2) = \left(\frac{\theta(k_1 - K_{F,a})}{m_b} + \frac{\theta(K_{F,b} - k_1)}{m_a} \right) \pi \delta(k_1 - k_2) + (\theta(k_1 - K_{F,a})\theta(K_{F,b} - k_2) + \theta(k_2 - K_{F,a})$$

$$\times \theta(K_{F,b} - k_1)) \left(\frac{k_1}{2} J_1(k_1, k_2) - \frac{k_2}{2} J_0(k_1, k_2) \right). \tag{A69}$$

Then we finally have

$$F_2 = -2 \left(\prod_{i=1}^{4} \int_0^{+\infty} \frac{dk_i}{2\pi} k_i \right) \sum_n \xi_{n1}^{-1}(\boldsymbol{0}, \omega) f_{10}(\omega; k_1) \tau(k_1, k_2) f_{n1}(\omega; k_2) f_{n1}(\omega; k_3) \tau(k_3, k_4) f_{10}(\omega; k_4). \tag{A70}$$

To evaluate Eq. (A70) numerically, we discretize k_i ($i = 1, 2, 3, 4$) as in Eq. (A16),

$$F_2 = -2 \sum_{k_1, k_2, k_3, k_4, n} \frac{V_{10, k_1}^{\omega} T_{k_1 k_2} V_{n1, k_2}^{\omega} V_{n1, k_3}^{\omega} T_{k_3 k_4} V_{10, k_4}^{\omega}}{\xi_{n1}(\boldsymbol{0}, \omega)} = -2 \sum_{k_1, k_2, k_3, k_4} V_{10, k_1}^{\omega} T_{k_1 k_2} H_{1, k_2 k_3}^{\omega, -1} T_{k_3 k_4} V_{10, k_4}^{\omega}. \tag{A71}$$

Here $V_{nm,k}^{\omega}$ and $H_{m,kk'}^{\omega}$ are defined in Eq. (A27) and

$$
T_{k_1 k_2} \equiv \frac{\sqrt{k_1 k_2}}{L} \tau(k_1, k_2) = k_1 \left(\frac{\theta(k_1 - K_{F,a})}{2m_b} + \frac{\theta(K_{F,b} - k_1)}{2m_a} \right) \delta_{k_1 k_2} + \frac{\sqrt{k_1 k_2}}{L}
$$
$$
\times \left(\theta(k_1 - K_{F,a}) \theta(K_{F,b} - k_2) + \theta(k_2 - K_{F,a}) \theta(K_{F,b} - k_1) \right) \left(\frac{k_1}{2} J_1(k_1, k_2) - \frac{k_2}{2} J_0(k_1, k_2) \right).
$$

S_1 in Eq. (A42) is given by the 2D momentum integrals,

$$
S_1 = \sum_{\mathbf{k}_1, \mathbf{k}_2} \langle \phi_{10}(\mathbf{0}, \omega) | \mathbf{k}_1 \rangle [S_x]_{k_1 k_2} \langle \mathbf{k}_2 | \phi_{10}(\mathbf{0}, \omega) \rangle = \frac{1}{2} \sum_{\mathbf{k}_1, \mathbf{k}_2} \langle \phi_{10}(\mathbf{0}, \omega) | \mathbf{k}_1 \rangle [S_x + S_y]_{k_1 k_2} \langle \mathbf{k}_2 | \phi_{10}(\mathbf{0}, \omega) \rangle
$$
$$
= \left(\prod_{i=1}^{2} \int_0^{+\infty} \frac{dk_i}{2\pi} \, k_i \int_0^{2\pi} \frac{d\varphi_i}{2\pi} \right) f_{10}(\omega; k_1) \Omega S(\mathbf{k_1}, \mathbf{k_2}) f_{10}(\omega; k_2). \tag{A72}
$$

$\Omega S = \frac{\Omega}{2}(S_x + S_y)$ is further expanded in terms of the Fourier series,

$$
\Omega S(\mathbf{k_1}, \mathbf{k_2}) = \left(-\frac{\theta(k_1 - K_{F,a})}{m_b} + \frac{\theta(K_{F,b} - k_1)}{m_a} \right) \frac{\pi \delta(k_1 - k_2)}{k_1} \sum_m e^{im(\varphi_1 - \varphi_2)}
$$
$$
+ \left(\theta(k_1 - K_{F,a}) \theta(K_{F,b} - k_2) + \theta(k_2 - K_{F,a}) \theta(K_{F,b} - k_1) \right) \sum_m K_m(k_1, k_2) e^{im(\varphi_1 - \varphi_2)}, \tag{A73}
$$

with Fourier coefficients

$$
K_m(k_1, k_2) = \frac{1}{2} \int_0^{2\pi} \frac{d(\varphi_1 - \varphi_2)}{2\pi} e^{-im(\varphi_1 - \varphi_2)} \left\{ \frac{2\pi}{\left(\sqrt{k_1^2 + k_2^2 - 2k_1 k_2 \cos(\varphi_1 - \varphi_2)} + k_{TF} \right)^3} \right.
$$
$$
\left. - \frac{\pi}{\left(\sqrt{k_1^2 + k_2^2 - 2k_1 k_2 \cos(\varphi_1 - \varphi_2)} + k_{TF} \right)^2} \frac{1}{\sqrt{k_1^2 + k_2^2 - 2k_1 k_2 \cos(\varphi_1 - \varphi_2)}} \right\}. \tag{A74}
$$

After the integrals over φ_1 and φ_2 in Eq. (A72), only the $m = 0$ term in Eq. (A73) remains finite,

$$
S_1 = \left(\prod_{i=1}^{2} \int_0^{+\infty} \frac{dk_i}{2\pi} \, k_i \right) f_{10}(\omega; k_1) \chi(k_1, k_2) f_{10}(\omega; k_2), \tag{A75}
$$

with

$$
\chi(k_1, k_2) = \left(-\frac{\theta(k_1 - K_{F,a})}{m_b} + \frac{\theta(K_{F,b} - k_1)}{m_a} \right) \frac{\pi \delta(k_1 - k_2)}{k_1} + \left(\theta(k_1 - K_{F,a}) \theta(K_{F,b} - k_2) \right.
$$
$$
\left. + \theta(k_2 - K_{F,a}) \theta(K_{F,b} - k_1) \right) \times K_0(k_1, k_2). \tag{A76}
$$

To evaluate Eq. (A75) numerically, we put it in a discrete form

$$
S_1 = \sum_{k_1, k_2} V_{10,k_1}^{\omega} X_{k_1 k_2} V_{10,k_2}^{\omega}, \tag{A77}
$$

where $V_{nm,k}^{\omega}$ are defined in Eq. (A27) and

$$
X_{k_1 k_2} = \frac{\sqrt{k_1 k_2}}{L} \chi(k_1, k_2) = \left(-\frac{\theta(k_1 - K_{F,a})}{2m_b} + \frac{\theta(K_{F,b} - k_1)}{2m_a} \right) \delta_{k_1 k_2}
$$
$$
+ \frac{\sqrt{k_1 k_2}}{L} \times \left(\theta(k_1 - K_{F,a}) \theta(K_{F,b} - k_2) + \theta(k_2 - K_{F,a}) \theta(K_{F,b} - k_1) \right) \times K_0(k_1, k_2). \tag{A78}
$$

In summary, $b_j(\omega)$ is given by Eqs. (A42), (A71), and (A77) evaluated at $\omega = \pm \omega_{\pm}$. The energy-band curvatures of exciton and antiexciton bands are obtained by Eqs. (A62) and (A63).

We can see from the expression in Eq. (A42) that the F_2 term is always positive. Our numerical calculation shows that, in the parameter regions we studied, the F_2 term dominates over the S_1 term, which makes $b_j(\omega_+)$ and $b_j(-\omega_-)$ always positive. Thus, from Eq. (A63), we can see that the band curvatures around the Γ point become negative. In Fig. 6, we show the values of the band curvatures as we vary the electron mass $\bar{m}$ ($m_a = m_b$) and fix E_g and μ.

APPENDIX B: "ANTIPARTICLE OF AN EXCITON" IN PREVIOUS LITERATURE

"Antiexciton" had been introduced in previous theoretical literature with different definitions [17,18,20,21]. In the following two sections, we clarify the physical difference between our concept of the antiexciton and those in the literature.

1. "Antiparticle of an exciton" that is an identical entity to its own counterpart exciton

Unlike the antiexciton proposed in this paper, the "antiexciton" introduced in some literature [17,18] characterizes the *same* interband collective mode as its own counterpart exciton. References [17,18] studied generic semiconductors without the U(1)×U(1) symmetry. An effective exciton Hamiltonian in such a system has no U(1) symmetry and the two-particle Green's function has pairs of a positive-energy pole and a negative-energy pole that are related to each other by a generic particle-hole symmetry of the effective exciton Hamiltonian. The literature [17,18] defines such pairs of a positive-energy pole and a negative-energy pole as excitons and their antiparticle counterparts ("antiexcitons"), respectively. In this section, we will show that the negative-energy pole related to the positive-energy pole by the generic particle-hole symmetry is redundant and the two poles characterize an identical physical excitation.

In the following, we first explain a generic particle-hole symmetry of a free boson Hamiltonian. The symmetry relates a pair of a positive-energy eigenstate and a negative-energy eigenstate, while the two "states" actually characterize an identical physical state. To see this point in a simple way, let us begin with a general Bogoliubov–de Gennes (BdG) Hamiltonian for free boson systems. For a later comparison to the Bethe-Salpeter equation for excitons, we assume the spatial translational symmetry, while the following argument can be easily generalized into the other cases without the translational symmetry. The Hamiltonian in the momentum space reads

$$\mathcal{H} = \frac{1}{2} \sum_{q} (\boldsymbol{\gamma}_q^\dagger \quad \boldsymbol{\gamma}_{-q}) \begin{pmatrix} A(q) & B(q) \\ B^*(-q) & A^*(-q) \end{pmatrix} \begin{pmatrix} \boldsymbol{\gamma}_q \\ \boldsymbol{\gamma}_{-q}^\dagger \end{pmatrix}$$

$$\equiv \frac{1}{2} \sum_{q} (\boldsymbol{\gamma}_q^\dagger \quad \boldsymbol{\gamma}_{-q}) H_{\text{BdG}}(q) \begin{pmatrix} \boldsymbol{\gamma}_q \\ \boldsymbol{\gamma}_{-q}^\dagger \end{pmatrix}. \tag{B1}$$

Here $\boldsymbol{\gamma}_q^\dagger$ ($\boldsymbol{\gamma}_{-q}$) is an m-component vector of boson creation (annihilation) operators with a momentum q ($-q$), e.g.,

$$(\boldsymbol{\gamma}_q^\dagger \quad \boldsymbol{\gamma}_{-q}) \equiv (\gamma_{1,q}^\dagger \quad \cdots \quad \gamma_{m,q}^\dagger \quad \gamma_{1,-q} \quad \cdots \quad \gamma_{m,-q}). \tag{B2}$$

Each component of the creation and annihilation operators obeys the commutation relations, e.g., $[\gamma_{j,q}, \gamma_{m,q'}^\dagger] = \delta_{j,m}\delta_{q,q'}$. The boson's commutation relation leads to $B^T(-q) = B(q)$. The Hermiticity of $\mathcal{H}$ results in the Hermiticity of the $m \times m$ matrix $A(q)$ [$A(q) = A^\dagger(q)$] as well as a following generic

symmetry of the $2m \times 2m$ matrix $H_{\text{BdG}}(q)$,

$$\sigma_1 H_{\text{BdG}}(q) \sigma_1 = \begin{pmatrix} A^*(-q) & B^*(-q) \\ B(q) & A(q) \end{pmatrix}$$

$$= H_{\text{BdG}}^*(-q). \tag{B3}$$

Here σ_1 exchanges $\boldsymbol{\gamma}_{-q}^\dagger$ (particle) and $\boldsymbol{\gamma}_q$ (hole), so that we dub this symmetry the particle-hole symmetry. Unlike the particle-hole symmetry for a many-body Hamiltonian [1], the particle-hole symmetry here is only due to the Hermiticity of $\mathcal{H}$ and the boson's commutation relation. Thus, any free boson Hamiltonians have this particle-hole symmetry in some bases (e.g., see below for an effective exciton Hamiltonian). To emphasize this point, we call this symmetry a *generic* particle-hole symmetry.

The BdG Hamiltonian is diagonalized by a Bogoliubov transformation T,

$$T^\dagger H_{\text{BdG}}(q) T = \begin{pmatrix} E(q) & \\ & E(-q) \end{pmatrix},$$

$$\begin{pmatrix} \boldsymbol{\gamma}_q \\ \boldsymbol{\gamma}_{-q}^\dagger \end{pmatrix} = T \begin{pmatrix} \eta_q \\ \eta_{-q}^\dagger \end{pmatrix}. \tag{B4}$$

$E(q)$ is a diagonal matrix whose diagonal elements are eigenenergies of new boson fields η_q with the momentum q,

$$\mathcal{H} = \frac{1}{2} \sum_{q} \sum_{j=1}^{m} (E_j(q) \eta_{j,q}^\dagger \eta_{j,q} + E_j(-q) \eta_{j,-q} \eta_{j,-q}^\dagger). \tag{B5}$$

To connect the commutation relations among the old boson fields with the commutation relations among the new boson fields, the Bogoliubov transformation must satisfy the paraunitarity condition,

$$T^\dagger \sigma_3 T = T \sigma_3 T^\dagger = \sigma_3. \tag{B6}$$

σ_3 in the equation is a 2×2 diagonal Pauli matrix, taking $+1$ in the hole space ($\boldsymbol{\gamma}_q$ or η_q) and -1 in the particle space ($\boldsymbol{\gamma}_{-q}^\dagger$ or $\eta_{-q}^\dagger$). With the commutation relation of the new boson fields, we have $\mathcal{H} = \sum_{q,j} E_j(q) \eta_{j,q}^\dagger \eta_{j,q} + \text{const}$.

To facilitate a later comparison to the Bethe-Salpeter equation for the interband excitations, let us next derive an equation of motion of the free boson systems. The equation of motion for the free boson fields takes the form of a generalized Hermitian eigenvalue problem,

$$i\sigma_3 \partial_t \begin{pmatrix} \boldsymbol{\gamma}_q \\ \boldsymbol{\gamma}_{-q}^\dagger \end{pmatrix} = H_{\text{BdG}}(q) \begin{pmatrix} \boldsymbol{\gamma}_q \\ \boldsymbol{\gamma}_{-q}^\dagger \end{pmatrix}, \tag{B7}$$

with $H_{\text{BdG}}(q) = H_{\text{BdG}}^\dagger(q)$. The diagonal Pauli matrix σ_3 on the left-hand side comes from the boson's commutation relations, $[\gamma_{i,q}, \gamma_{j,q}^\dagger] = -[\gamma_{i,q}^\dagger, \gamma_{j,q}] = \delta_{i,j}$.

The generic particle-hole symmetry of the BdG Hamiltonian [Eq. (B3)] formally relates a pair of positive-energy and negative-energy eigenmodes of the equation of motion. Suppose that the equation of motion has a solution Ψ of a positive energy ω and a momentum q as

$$\begin{pmatrix} \boldsymbol{\gamma}_q \\ \boldsymbol{\gamma}_{-q}^\dagger \end{pmatrix} = \Psi e^{-i\omega t} \tag{B8}$$

with $\omega\sigma_3\Psi = H_{\text{BdG}}(\boldsymbol{q})\Psi$. Such Ψ is a column vector of T for η_q in Eq. (B4). Then the particle-hole symmetry in Eq. (B3) formally relates this solution with a solution of the equation of motion at $-\boldsymbol{q}$ with a negative energy $-\omega$,

$$\begin{pmatrix} \boldsymbol{\gamma}_{-q} \\ \boldsymbol{\gamma}_q^\dagger \end{pmatrix} = \sigma_1\Psi^* e^{i\omega t}. \qquad (B9)$$

Namely, $-\omega\sigma_3(\sigma_1\Psi^*) = H_{\text{BdG}}(-\boldsymbol{q})(\sigma_1\Psi^*)$. These two solutions clearly describe an identical interband collective mode, because the Hermitian conjugate of Eq. (B8) is nothing but Eq. (B9).

In the following, we will review previous theories, where the Bethe-Salpeter equation for the two-particle Green's function always reduces to a generalized Hermitian eigenvalue problem of Eq. (B7) together with a BdG-type Hamiltonian [3,4,17,18]. The BdG Hamiltonian is nothing but a free boson Hamiltonian of excitons (more generally, interband excitations), and it has a generic particle-hole symmetry in a certain basis. The symmetry comes from the Hermiticity of an original many-body Hamiltonian of electrons and bosonic nature of excitons. In this sense, it is equivalent to Eq. (B3). Due to the generic particle-hole symmetry, the Green's function formally has pairs of a positive-energy pole (ω) at $\boldsymbol{q}$ and a negative-energy pole ($-\omega$) at $-\boldsymbol{q}$ that are connected to each other by the symmetry. Some literature [17,18] defines the positive-energy pole at ω and the negative-energy pole ($-\omega$) as exciton and its antiparticle counterpart ("antiexciton"), re-

spectively. However, the two poles characterize exactly an identical physical eigenmode as in Eqs. (B8) and (B9).

To show this more explicitly, we follow Glutsch and Bechstedt's papers [17,18] and add an interband hopping term into a two-band system:

$$\hat{H} = \hat{H}_0 + \hat{V},$$

$$\hat{H}_0 = \sum_{\boldsymbol{k}} [\epsilon_a(\boldsymbol{k})a_{\boldsymbol{k}}^\dagger a_{\boldsymbol{k}} + \epsilon_b(\boldsymbol{k})b_{\boldsymbol{k}}^\dagger b_{\boldsymbol{k}} + \Delta(\boldsymbol{k})a_{\boldsymbol{k}}^\dagger b_{\boldsymbol{k}} + \Delta^*(\boldsymbol{k})b_{\boldsymbol{k}}^\dagger a_{\boldsymbol{k}}],$$

$$(B10)$$

where $\hat{V}$ is the same as Eq. (3). The interband hopping term $\Delta(\boldsymbol{k})$ can come from an intrinsic band hybridization [3,4], an external pump field [17,18], or spontaneous symmetry breaking by exciton condensation [20,21]. When a Fermi level is placed inside a band gap (see below), the Hamiltonian describes a generic semiconductor without the U(1)×U(1) symmetry. $a_{\boldsymbol{k}} = u(\boldsymbol{k})\alpha_{\boldsymbol{k}} + v(\boldsymbol{k})\beta_{\boldsymbol{k}}$, $b_{\boldsymbol{k}} = -v^*(\boldsymbol{k})\alpha_{\boldsymbol{k}} + u(\boldsymbol{k})\beta_{\boldsymbol{k}}$ with $|u(\boldsymbol{k})|^2 + |v(\boldsymbol{k})|^2 = 1$,

$$\hat{H}_0 = \sum_{\boldsymbol{k}}[\Omega_+(\boldsymbol{k})\alpha_{\boldsymbol{k}}^\dagger\alpha_{\boldsymbol{k}} + \Omega_-(\boldsymbol{k})\beta_{\boldsymbol{k}}^\dagger\beta_{\boldsymbol{k}}],$$

with

$$\Omega_\pm(\boldsymbol{k}) \equiv \frac{\epsilon_a(\boldsymbol{k}) + \epsilon_b(\boldsymbol{k})}{2} \pm \frac{\sqrt{(\epsilon_a(\boldsymbol{k}) - \epsilon_b(\boldsymbol{k}))^2 + 4|\Delta(\boldsymbol{k})|^2}}{2}. \qquad (B11)$$

In terms of interaction between α and β fermions, the interaction part is given by

$$\hat{V} = \frac{1}{2\Omega}\sum_{\boldsymbol{q},\boldsymbol{k},\boldsymbol{k}'}(2A_{\boldsymbol{k},\boldsymbol{k}'}(\boldsymbol{q})\alpha_{\boldsymbol{k}+\boldsymbol{q}}^\dagger\beta_{\boldsymbol{k}'}^\dagger\beta_{\boldsymbol{k}}\alpha_{\boldsymbol{k}'+\boldsymbol{q}} + B_{\boldsymbol{k},\boldsymbol{k}'}(\boldsymbol{q})\alpha_{\boldsymbol{k}+\boldsymbol{q}}^\dagger\alpha_{-\boldsymbol{k}'-\boldsymbol{q}}^\dagger\beta_{\boldsymbol{k}}\beta_{-\boldsymbol{k}'} + B_{-\boldsymbol{k},-\boldsymbol{k}'}^*(-\boldsymbol{q})\beta_{-\boldsymbol{k}}^\dagger\beta_{\boldsymbol{k}'}^\dagger\alpha_{-\boldsymbol{k}-\boldsymbol{q}}\alpha_{\boldsymbol{k}'+\boldsymbol{q}}) + \cdots$$

$$= \frac{1}{2\Omega}\sum_{\boldsymbol{q},\boldsymbol{k},\boldsymbol{k}'}(2A_{-\boldsymbol{k},-\boldsymbol{k}'}^*(-\boldsymbol{q})\beta_{-\boldsymbol{k}}^\dagger\alpha_{-\boldsymbol{k}'-\boldsymbol{q}}^\dagger\alpha_{-\boldsymbol{k}-\boldsymbol{q}}\beta_{\boldsymbol{k}'} + B_{\boldsymbol{k},\boldsymbol{k}'}(\boldsymbol{q})\alpha_{\dots}^\dagger\alpha_{\dots}^\dagger\beta_{\dots}\beta_{\dots} + B_{-\boldsymbol{k},-\boldsymbol{k}'}^*(-\boldsymbol{q})\beta_{\dots}^\dagger\beta_{\dots}^\dagger\alpha_{\dots}\alpha_{\dots}) + \cdots, \qquad (B12)$$

where matrix elements of $A(\boldsymbol{q})$ and $B(\boldsymbol{q})$ are given by the unitary transformation; "$\cdots$" on the right-hand sides are those terms that take forms of either $\alpha^\dagger\alpha^\dagger\alpha\alpha$ or $\beta^\dagger\beta^\dagger\beta\beta$, while they do not contribute to the BS equation in a semiconductor region considered below. Note that the Hermiticity of $\hat{V}$ requires $A_{\boldsymbol{k},\boldsymbol{k}'}(\boldsymbol{q}) = A_{\boldsymbol{k}',\boldsymbol{k}}^*(\boldsymbol{q})$, and relates the matrix elements of the second term ($\alpha^\dagger\alpha^\dagger\beta\beta$) and the third term ($\beta^\dagger\beta^\dagger\alpha\alpha$) as in the equation. With the sum over $\boldsymbol{q}$, $\boldsymbol{k}$, and $\boldsymbol{k}'$, we can always symmetrize $B(\boldsymbol{q})$ such that $B_{\boldsymbol{k},\boldsymbol{k}'}(\boldsymbol{q}) = B_{-\boldsymbol{k}',-\boldsymbol{k}}(-\boldsymbol{q})$.

Following the papers [17,18], we consider that $\Delta(\boldsymbol{k})$ results in a direct gap between the α band and β band, and we place a chemical potential μ inside the energy gap: $\Omega_+(\boldsymbol{k}) > \mu > \Omega_-(\boldsymbol{k})$ for all the $\boldsymbol{k}$. A many-body ground state $|0\rangle$ is considered to be adiabatically connected to this semiconductor ground state. The interband collective modes above the many-body ground state can be analyzed by an interband two-particle Green's function, which generally takes a 2×2 matrix form,

$$\hat{\mathcal{G}}^{ex}(\boldsymbol{x} - \boldsymbol{x}', t - t')_{yy'} \equiv -(-i)^2\begin{pmatrix} \langle 0|\mathcal{T}\{\gamma(\boldsymbol{x}, \boldsymbol{y}; t)\gamma^\dagger(\boldsymbol{x}', \boldsymbol{y}'; t')\}|0\rangle & \langle 0|\mathcal{T}\{\gamma(\boldsymbol{x}, \boldsymbol{y}, t)\gamma(\boldsymbol{x}', \boldsymbol{y}'; t')\}|0\rangle \\ \langle 0|\mathcal{T}\{\gamma^\dagger(\boldsymbol{x}, \boldsymbol{y}, t)\gamma^\dagger(\boldsymbol{x}', \boldsymbol{y}', t')\}|0\rangle & \langle 0|\mathcal{T}\{\gamma^\dagger(\boldsymbol{x}, \boldsymbol{y}, t)\gamma(\boldsymbol{x}', \boldsymbol{y}', t')\}|0\rangle \end{pmatrix}, \qquad (B13)$$

with $\gamma(\boldsymbol{x}, \boldsymbol{y}; t) \equiv \alpha_{\boldsymbol{x}}(t)\beta_{\boldsymbol{x}+\boldsymbol{y}}^\dagger(t)$ and $\gamma^\dagger(\boldsymbol{x}, \boldsymbol{y}; t) \equiv \beta_{\boldsymbol{x}+\boldsymbol{y}}(t)\alpha_{\boldsymbol{x}}^\dagger(t)$. The t dependence of the operators is in the Heisenberg picture. $\gamma(\boldsymbol{x}, \boldsymbol{y})$ and $\gamma^\dagger(\boldsymbol{x}, \boldsymbol{y})$ can be regarded as annihilation and creation of excitons, respectively. Note that the $\alpha^\dagger\alpha^\dagger\beta\beta$ and $\beta^\dagger\beta^\dagger\alpha\alpha$ terms in $\hat{V}$ break a U(1) symmetry of $\alpha \to \alpha e^{i\theta}$ and $\beta \to \beta e^{-i\theta}$. Thereby, the interband Green's function generally takes the 2×2 matrix form in the particle-hole space of the exciton fields.

After Fourier transforms of the spatial coordinates, the Green's function is given by a function of a momentum $\boldsymbol{q}$ of the center-of-mass coordinate between two fermions and momenta $\boldsymbol{k}$, $\boldsymbol{k}'$ of the relative coordinates,

$$\hat{\mathcal{G}}^{ex}(\boldsymbol{q}, t - t')_{\boldsymbol{k}\boldsymbol{k}'} \equiv \int d^d(\boldsymbol{x} - \boldsymbol{x}')\int d^d\boldsymbol{y}\int d^d\boldsymbol{y}' e^{-i\boldsymbol{q}\cdot(\boldsymbol{x}-\boldsymbol{x}')+i\boldsymbol{k}\cdot\boldsymbol{y}-i\boldsymbol{k}'\cdot\boldsymbol{y}'}\hat{\mathcal{G}}^{ex}(\boldsymbol{x} - \boldsymbol{x}', t - t')_{yy'}, \qquad (B14)$$

with

$$\hat{\mathcal{G}}^{ex}(\boldsymbol{q}, t-t')_{kk'} = -(-i)^2 \Omega \begin{pmatrix} \langle 0|\mathcal{T}\{\alpha_{k+q}(t)\beta_k^\dagger(t)\beta_{k'}(t')\alpha_{k'+q}^\dagger(t')\}|0\rangle & \langle 0|\mathcal{T}\{\alpha_{k+q}(t)\beta_k^\dagger(t)\alpha_{-k'-q}(t')\beta_{-k'}^\dagger(t')\}|0\rangle \\ \langle 0|\mathcal{T}\{\beta_{-k}(t)\alpha_{-k-q}^\dagger(t)\beta_{k'}(t')\alpha_{k'+q}^\dagger(t')\}|0\rangle & \langle 0|\mathcal{T}\{\beta_{-k}(t)\alpha_{-k-q}^\dagger(t)\alpha_{-k'-q}(t')\beta_{-k'}^\dagger(t')\}|0\rangle \end{pmatrix}. \quad \text{(B15)}$$

Here Ω is the system volume.

The ground state in the noninteracting limit is a vacuum of α and $\beta^\dagger$, $\alpha|0\rangle_{V=0} = \beta^\dagger|0\rangle_{V=0} = 0$, where the interband Green's function takes a diagonal form in the particle-hole space,

$$\hat{\mathcal{G}}_0^{ex}(\boldsymbol{q}, t-t')_{kk'} = \Omega\delta_{k,k'} \begin{pmatrix} \theta(t-t')e^{-i(\Omega_+(k+q)-\Omega_-(k))(t-t')} & 0 \\ 0 & \theta(t'-t)e^{i(\Omega_+(-k-q)-\Omega_-(-k))(t-t')} \end{pmatrix}. \quad \text{(B16)}$$

In the presence of $\hat{V}$ of Eq. (B12), the interband two-particle Green's function is given by a solution of the following Bethe-Salpeter equation:

$$\hat{\mathcal{G}}^{ex}(\boldsymbol{q}, t-t')_{kk'} = \hat{\mathcal{G}}_0^{ex}(\boldsymbol{q}, t-t')_{kk'} + \frac{i}{\Omega^2}\sum_{\bar{k},\bar{k}'}\int d\bar{t}\, \hat{\mathcal{G}}_0^{ex}(\boldsymbol{q}, t-\bar{t})_{k\bar{k}} \begin{pmatrix} A_{\bar{k},\bar{k}'}(\boldsymbol{q}) & B_{\bar{k},\bar{k}'}(\boldsymbol{q}) \\ B_{-\bar{k},-\bar{k}'}^*(-\boldsymbol{q}) & A_{-\bar{k},-\bar{k}'}^*(-\boldsymbol{q}) \end{pmatrix} \hat{\mathcal{G}}^{ex}(\boldsymbol{q}, \bar{t}-t')_{\bar{k}'k'}. \quad \text{(B17)}$$

After the Fourier transform in time, the equation reduces to a generalized Hermitian eigenvalue problem with a BdG-type Hamiltonian $\boldsymbol{H}_{\text{BdG}}(\boldsymbol{q})$:

$$\sum_{\bar{k}}(\delta_{k,\bar{k}}(\omega\sigma_3 + i0^+\sigma_0) - \boldsymbol{H}_{\text{BdG}}(\boldsymbol{q})_{k,\bar{k}})\widetilde{\mathcal{G}}^{ex}(\boldsymbol{q}, \omega)_{\bar{k},k'} = \delta_{k,k'}\sigma_0, \quad \text{(B18)}$$

with $\boldsymbol{H}_{\text{BdG}}(\boldsymbol{q}) = \boldsymbol{H}_{\text{BdG}}^\dagger(\boldsymbol{q})$. Here the Green's function is normalized by $i\Omega$, $i\Omega\widetilde{\mathcal{G}}^{ex} \equiv \hat{\mathcal{G}}^{ex}$. The BdG Hamiltonian is a free boson Hamiltonian of excitons (interband excitations) and it takes a 2×2 matrix form in the particle-hole space of the exciton fields,

$$\boldsymbol{H}_{\text{BdG}}(\boldsymbol{q})_{k,k'} = \delta_{k,k'} \begin{pmatrix} \Omega_+(\boldsymbol{k}+\boldsymbol{q}) - \Omega_-(\boldsymbol{k}) & \\ & \Omega_+(-\boldsymbol{k}-\boldsymbol{q}) - \Omega_-(-\boldsymbol{k}) \end{pmatrix} - \frac{1}{\Omega} \begin{pmatrix} A_{k,k'}(\boldsymbol{q}) & B_{k,k'}(\boldsymbol{q}) \\ B_{-k,-k'}^*(-\boldsymbol{q}) & A_{-k,-k'}^*(-\boldsymbol{q}) \end{pmatrix}. \quad \text{(B19)}$$

σ_3 on the left-hand side of Eq. (B18) is the diagonal Pauli matrix taking $+1$ for the hole space of the exciton field (γ) and -1 for the particle space of the exciton field ($\gamma^\dagger$). $\omega\sigma_3$ is nothing but a Fourier transform of $i\sigma_3\partial_t$ on the left-hand side of Eq. (B7), standing for the boson's commutation relations of exciton fields. Thus, solving this Bethe-Salpeter equation of Eq. (B18) is essentially equivalent to solving the equation of motion of Eq. (B7).

The eigenvalue problem can be solved in terms of the parauniatry transformation. Suppose that the BdG Hamiltonian is diagonalized by a parauniatry transformation of Eq. (B4). Thereby, the diagonal elements in $\boldsymbol{E}(\boldsymbol{q})$ of Eq. (B4) are nothing but excitation energies of interband collective and individual excitations with the momentum $\boldsymbol{q}$. Column vectors in $\boldsymbol{T}$ of Eq. (B4) stand for wave functions of these eigenmodes. Due to the particle-hole mixing nature of $\boldsymbol{H}_{\text{BdG}}(\boldsymbol{q})$, $\boldsymbol{T}$ thus introduced comprises of both the hole-type wave functions for $\eta_{j,q}$ and the particle-type wave functions for $\eta_{j,-q}^\dagger$. We dub them $\boldsymbol{\Psi}_j$ and $\boldsymbol{\Phi}_j$, respectively ($j = 1, 2, \dots$):

$$\boldsymbol{T} \equiv (\boldsymbol{\Psi}_1 \quad \boldsymbol{\Psi}_2 \quad \cdots \boldsymbol{\Phi}_1 \quad \boldsymbol{\Phi}_2 \quad \cdots). \quad \text{(B20)}$$

$\boldsymbol{\Psi}_j$ for $\eta_{j,q}$ here corresponds to $\boldsymbol{\Psi}$ in Eq. (B8). To preserve the boson statistics between $\eta_{j,q}$ and $\eta_{m,q}^\dagger$ of Eq. (B4), these wave functions are normalized with the parauniatry condition of Eq. (B6). The orthonormalization is given by $\boldsymbol{\Psi}_m^\dagger\sigma_3\boldsymbol{\Psi}_j = \delta_{j,m}$, $\boldsymbol{\Phi}_m^\dagger\sigma_3\boldsymbol{\Phi}_j = -\delta_{j,m}$, and $\boldsymbol{\Psi}_m^\dagger\sigma_3\boldsymbol{\Phi}_j = \boldsymbol{\Phi}_m^\dagger\sigma_3\boldsymbol{\Psi}_j = 0$ ($j, m = 1, 2, \dots$). The completeness relation is defined by

$$\boldsymbol{T}\sigma_3\boldsymbol{T}^\dagger = \sum_j \boldsymbol{\Psi}_{j,k}\boldsymbol{\Psi}_{j,k'}^* - \sum_j \boldsymbol{\Phi}_{j,k}\boldsymbol{\Phi}_{j,k'}^* = \sigma_3\delta_{k,k'}. \quad \text{(B21)}$$

With these orthogonality and completeness relations, Eq. (B4) can be rewritten into

$$\boldsymbol{H}_{\text{BdG}}(\boldsymbol{q})\boldsymbol{\Psi}_j = \sigma_3\boldsymbol{\Psi}_j E_j(\boldsymbol{q}),$$
$$\boldsymbol{H}_{\text{BdG}}(\boldsymbol{q})\boldsymbol{\Phi}_j = -\sigma_3\boldsymbol{\Phi}_j E_j(-\boldsymbol{q}), \quad \text{(B22)}$$

for $j = 1, 2, \dots$. Given the parauniatry transformation, the interband Green's function at $\boldsymbol{q}$ is obtained as a solution of the Bethe-Salpeter equation,

$$\widetilde{\mathcal{G}}^{ex}(\boldsymbol{q}, \omega)_{k,k'} = \sum_j \frac{\boldsymbol{\Psi}_{j,k}\boldsymbol{\Psi}_{j,k'}^*}{\omega - E_j(\boldsymbol{q}) + i0^+}$$
$$- \sum_j \frac{\boldsymbol{\Phi}_{j,k}\boldsymbol{\Phi}_{j,k'}^*}{\omega + E_j(-\boldsymbol{q}) - i0^+}. \quad \text{(B23)}$$

Note that, thanks to the completeness relation of Eq. (B21), the solution satisfies a sum rule,

$$\int_{-\infty}^{+\infty} \frac{d\omega}{2\pi i}\widetilde{\mathcal{G}}^{ex}(\boldsymbol{q}, \omega)_{k,k'}(e^{-i\omega 0^+} - e^{i\omega 0^+}) = \sigma_3\delta_{k,k'}. \quad \text{(B24)}$$

The sum rule is a boundary condition in time, $i\widetilde{\mathcal{G}}(\boldsymbol{q}, t = 0+) - i\widetilde{\mathcal{G}}(\boldsymbol{q}, t = 0-) = \sigma_3\delta_{k,k'}$. One can obtain the boundary condition by noting $\langle 0|\alpha_k^\dagger\alpha_k|0\rangle = 0$ and $\langle 0|\beta_k^\dagger\beta_k|0\rangle = 1$. Here $|0\rangle$ is the many-body ground state.

Like in the free boson system, the BdG Hamiltonian of excitons, $\boldsymbol{H}_{\text{BdG}}(\boldsymbol{q})$, has a generic particle-hole symmetry in a certain basis:

$$\sigma_1\hat{\boldsymbol{H}}_{\text{BdG}}^*(\boldsymbol{q})_{k,k'}\sigma_1 = \hat{\boldsymbol{H}}_{\text{BdG}}(-\boldsymbol{q})_{-k,-k'}. \quad \text{(B25)}$$

As was explained below Eq. (B12), the symmetry comes from the Hermiticity of the original many-body Hamiltonian of electrons and the bosonic nature of excitons. Due to this generic symmetry, the BdG Hamiltonian $H_{\mathrm{BdG}}(-q)$ at $-q$ is diagonalized by the following paraunitary transformation:

$$\sigma_1 T^* \sigma_1 = (\sigma_1 \Phi_1^* \quad \sigma_1 \Phi_2^* \quad \cdots \sigma_1 \Psi_1^* \quad \sigma_1 \Psi_2^* \quad \cdots).$$
(B26)

This gives a solution of the interband Green's function at $-q$:

$$\widetilde{\mathcal{G}}^{ex}(-q,\omega)_{k,k'} = \sum_j \frac{\sigma_1 \Phi_{j,-k}^* \Phi_{j,-k'} \sigma_1}{\omega - E_j(-q) + i0^+}$$
$$- \sum_j \frac{\sigma_1 \Psi_{j,-k}^* \Psi_{j,-k'} \sigma_1}{\omega + E_j(q) - i0^+}.$$
(B27)

Some previous works [17,18] in the literature [3,4,17,18] defined the positive-energy poles at $\omega = E_j(q)$ as excitons and the negative-energy poles at $\omega = -E_j(-q)$ in Eq. (B23) as its counterpart "antiexcitons," respectively. However, a comparison between Eq. (B23) and Eq. (B27) clearly shows that the negative-energy poles are completely redundant, because all the information of physical eigenmodes of the system is solely encoded in the positive-energy poles of *all* the q. In fact, as shown explicitly in the comparison between Eq. (B8) and Eq. (B9), the negative-energy poles at $-q$ with $\omega = -E_j(q)$ characterize the same physical excitation as the positive-energy poles at q with $\omega = E_j(q)$. The equivalence is nothing but the equivalence between $\eta_{j,q}$ in the first term of Eq. (B5) at q and $\eta_{j,q}^\dagger$ in the second term of Eq. (B5) at $-q$.

Unlike the "antiexciton" introduced in the literature [17,18], the $|n\rangle$ state (exciton) and the $|n'\rangle$ state (antiexciton) in Eq. (9) describe two *different* excited eigenstates of the two-band semimetal model. In fact, in the presence of the $U(1) \times U(1)$ symmetry, where the two-band semimetal model commutes with total electron numbers of the a band and the b band, the exciton state lives in a Hilbert space of $|N_a + 1, N_b - 1\rangle$, the antiexciton state lives in a Hilbert space of $|N_a - 1, N_b + 1\rangle$, and these two spaces are decoupled from each other in an exact diagonalization of the many-body Hamiltonian for the semimetal model. Here N_a and N_b are the total electron numbers of the a band and the b band, respectively, and the semimetal ground state $|0\rangle$ is in a Hilbert space of $|N_a, N_b\rangle$. Since $a^\dagger b$ creates such an exciton and annihilates such an antiexciton in the semimetal ground state, the Green's function of $G^{ex}(x - x', t - t')_{yy'} \equiv \langle 0 | \mathcal{T}\{a_x(t) b_{x+y}^\dagger(t) b_{x'+y'}(t') a_{x'}^\dagger(t')\} | 0 \rangle$ has a pole for the exciton state in the positive-ω region and a pole for the antiexciton state in the negative-ω region.

In summary, our paper proposed a pair of the exciton and antiexciton as two *distinct* excited eigenstates above the semimetal ground state. Physically speaking, our concept of the antiexciton should be distinguished from "antiexciton" in the literature [17,18], which actually describes an identical excited eigenstate as its counterpart exciton state.

In the presence of single-particle hybridization between the two bands, $\Delta a^\dagger b$, $N_a - N_b$ becomes no longer a quantum number, and excitons (interband collective modes in the Hilbert space of $|N_a + 1, N_b - 1\rangle$) and antiexcitons (interband collective modes in the Hilbert space of $|N_a - 1, N_b + 1\rangle$) will be hybridized in general. Thus, interband collective modes

in such two-band models are no longer classified in terms of the exciton or antiexciton proposed in our paper. Nonetheless, when the hybridization Δ is much smaller than an energy difference between original exciton and antiexciton states at $\Delta = 0$, two weakly hybridized interband collective modes can be approximately regarded as an exciton mode and an antiexciton mode. In this sense, our concept of the exciton and antiexciton still provides a useful picture for distinguishing the two types of interband collective modes in two-band semimetals even with the hybridization.

2. "Antiparticle of an exciton" that does not coexist with its counterpart exciton

Reference [20] introduced a concept of "antiexciton" in a two-dimensional (2D) electron-hole gas (EHG) under high magnetic field, which one could consider to share a similar physical picture as the antiexciton proposed in this paper. The concept was further cited in Ref. [21]. Under the magnetic field, the 2D EHG forms Landau levels (LLs) of an electron-type band and a hole-type band. Though Ref. [20] considers an effective interband hybridization by exciton condensation, the classification of interband collective modes for the $U(1) \times U(1)$ symmetric case at zero temperature is approximately applicable for their case.

When the lowest LL (LLL) of the electron band (a band) is higher than the LLL of the hole band (b band) in energy and the Fermi level is set to the middle between the two LLLs ("small-ρ limit"), an interband collective mode in such a positive-band-gap semiconductor regime is a bound state of a particle in the a band and a hole in the b band; the interband collective mode lives in a Hilbert space of $|N_a + 1, N_b - 1\rangle$ (here we consider that the ground is in a Hilbert space of $|N_a, N_b\rangle$ with $N_a \ll N_b$). When the LLL of the electron band is lower than the LLL of the hole band and the Fermi level is placed into the middle of the two LLLs ("small-$(1 - \rho)$ limit"), an interband collective mode in such a negative-band-gap semiconductor regime is a bound state of a hole in the a band and a particle in the b band; the collective mode lives in a Hilbert space of $|N_a - 1, N_b + 1\rangle$ (here we consider that the ground is in a Hilbert space of $|N_a, N_b\rangle$ with $N_a \gg N_b$). Lerner and Lozovik called the interband collective modes in these positive-band-gap and negative-band-gap semiconductor regimes excitons and antiexcitons, respectively, so the concept of the antiexciton proposed in our paper shares the similar physical picture as that of Lerner and Lozovik.

Nonetheless, unlike in the semimetal model studied in this paper, the excitons and antiexcitons in the 2D EHG under the field *do not coexist* inside the same 2D bulk. Excitons exist only in the small-ρ limit and antiexcitons exist in the small-$(1 - \rho)$ limit. Physically speaking, the band inversion can be induced by changing the magnetic field, so that these two limits are realized in two different regions of the magnetic field. On the contrary, our paper proposes the universal coexistence of excitons and antiexcitons in the same semimetallic bulk. The coexistence of a pair of excitons and antiexcitons leads to two distinct absorption peaks in optical spectroscopy experiments as well as a fertile excitonic analog of the electron-positron pair annihilation phenomenon. These physical consequences cannot be realized by a 2D EHG under high magnetic field.

[1] M. Srednicki, *Quantum Field Theory* (Cambridge University Press, Cambridge, UK, 2007)

[2] D. Griffiths, *Introduction to Elementary Particles* (John Wiley & Sons, New York, 2020)

[3] M. Rohlfing and S. G. Louie, Electron-hole excitations and optical spectra from first principles, Phys. Rev. B **62**, 4927 (2000).

[4] R. M. Martin, L. Reining, and D. M. Ceperley, *Interacting Electrons: Theory and Computational Approaches* (Cambridge University Press, Cambridge, UK, 2016).

[5] G. Strinati, Application of the Greens functions method to the study of the optical properties of semiconductors, Riv. Nuovo Cim. **11**, 1 (1988).

[6] S. Koch, M. Kira, G. Khitrova, and H. Gibbs, Semiconductor excitons in new light, Nat. Mater. **5**, 523 (2006).

[7] R. A. Kaindl, M. A. Carnahan, D. Hägele, R. Lövenich, and D. S. Chemla, Ultrafast terahertz probes of transient conducting and insulating phases in an electron-hole gas, Nature (London) **423**, 734 (2003).

[8] M. Kira, F. Jahnke, and S. W. Koch, Microscopic Theory of Excitonic Signatures in Semiconductor Photoluminescence, Phys. Rev. Lett. **81**, 3263 (1998).

[9] B. Halperin and T. Rice, The excitonic state at the semiconductor-semimetal transition, in *Solid State Physics* (Elsevier, AMsterdam, 1968), Vol. 21, pp. 115–192.

[10] B. I. Halperin and T. M. Rice, Possible anomalies at a semimetal-semiconductor transition, Rev. Mod. Phys. **40**, 755 (1968).

[11] A. N. Kozlov and L. A. Maksimov, The metal-dielectric divalent crystal phase transition, Sov. Phys. JETP-USSR **21**, 790 (1965).

[12] E. Hanamura and H. Haug, Condensation effects of excitons, Phys. Rep. **33**, 209 (1977).

[13] A. Kogar, M. S. Rak, S. Vig, A. A. Husain, F. Flicker, Y. I. Joe, L. Venema, G. J. MacDougall, T. C. Chiang, E. Fradkin, J. van Wezel, and P. Abbamonte, Signatures of exciton condensation in a transition metal dichalcogenide, Science **358**, 1314 (2017).

[14] D. Jérome, T. M. Rice, and W. Kohn, Excitonic insulator, Phys. Rev. **158**, 462 (1967).

[15] J. M. Blatt, K. W. Böer, and W. Brandt, Bose-Einstein condensation of excitons, Phys. Rev. **126**, 1691 (1962).

[16] P. B. Littlewood, P. R. Eastham, J. M. J. Keeling, F. M. Marchetti, B. D. Simons, and M. H. Szymanska, Models of coherent exciton condensation, J. Phys.: Condens. Matter **16**, S3597 (2004).

[17] S. Glutsch and F. Bechstedt, Exciton redshift for coherent pumping near the absorption edge, Phys. Rev. B **44**, 1368 (1991).

[18] F. Bechstedt and S. Glutsch, Nonperturbative treatment of excitons in semiconductors coherently pumped near the absorption edge, Phys. Rev. B **44**, 3638 (1991).

[19] P. Arseev and A. Dzyubenko, Exciton magnetotransport in two-dimensional systems: Weak-localization effects, J. Exp. Theor. Phys. **87**, 200 (1998).

[20] I. V. Lerner and Y. E. Lozovik, Two-dimensional electron-hole system in a strong magnetic field as an almost ideal exciton gas, Zh. Eksp. Teor. Fiz. **80**, 1488 (1981).

[21] Y. E. Lozovik, O. L. Berman, and V. G. Tsvetus, Phase transitions of electron-hole and unbalanced electron systems in coupled quantum wells in high magnetic fields, Phys. Rev. B **59**, 5627 (1999).

[22] J. D. Cloizeaux, Exciton instability and crystallographic anomalies in semiconductors, J. Phys. Chem. Solids **26**, 259 (1965).

[23] A. L. Fetter and J. D. Walecka, *Quantum Theory of Many-Particle Systems* (Dover, New York, 2003).

[24] D. Pekker and C. Varma, Amplitude/Higgs modes in condensed matter physics, Annu. Rev. Condens. Matter Phys. **6**, 269 (2015).

[25] P. B. Littlewood and C. M. Varma, Gauge-Invariant Theory of the Dynamical Interaction of Charge Density Waves and Superconductivity, Phys. Rev. Lett. **47**, 811 (1981).

[26] P. B. Littlewood and C. M. Varma, Amplitude collective modes in superconductors and their coupling to charge-density waves, Phys. Rev. B **26**, 4883 (1982).

[27] C. Varma, Higgs boson in superconductors, J. Low Temp. Phys. **126**, 901 (2002).

[28] A. Altland and B. D. Simons, *Condensed Matter Field Theory*, 2nd ed. (Cambridge University Press, Cambridge, UK, 2010).

[29] M. Maialle and L. Sham, Exciton spin dynamics and polarized luminescence in quantum wells, Surf. Sci. **305**, 256 (1994).

[30] X.-X. Zhang, Y. You, S. Y. F. Zhao, and T. F. Heinz, Experimental Evidence for Dark Excitons in Monolayer WSe$_2$, Phys. Rev. Lett. **115**, 257403 (2015).

[31] G. Giuliani and G. Vignale, *Quantum Theory of the Electron Liquid* (Cambridge University Press, Cambridge, UK, 2005).

[32] B. Mihaila, Lindhard function of a d-dimensional Fermi gas, arXiv:1111.5337.

[33] A. Jain, S. P. Ong, G. Hautier, W. Chen, W. D. Richards, S. Dacek, S. Cholia, D. Gunter, D. Skinner, G. Ceder, and K. A. Persson, The Materials Project: A materials genome approach to accelerating materials innovation, APL Mater. **1**, 011002 (2013).

[34] X. Wu, W. Lou, K. Chang, G. Sullivan, and R.-R. Du, Resistive signature of excitonic coupling in an electron-hole double layer with a middle barrier, Phys. Rev. B **99**, 085307 (2019).

[35] Y. Jiang, S. Thapa, G. D. Sanders, C. J. Stanton, Q. Zhang, J. Kono, W. K. Lou, K. Chang, S. D. Hawkins, J. F. Klem, W. Pan, D. Smirnov, and Z. Jiang, Probing the semiconductor to semimetal transition in InAs/GaSb double quantum wells by magneto-infrared spectroscopy, Phys. Rev. B **95**, 045116 (2017).

[36] L. Du, X. Li, W. Lou, G. Sullivan, K. Chang, J. Kono, and R.-R. Du, Evidence for a topological excitonic insulator in InAs/GaSb bilayers, Nat. Commun. **8**, 1 (2017).

[37] J. Li, T. Taniguchi, K. Watanabe, J. Hone, and C. Dean, Excitonic superfluid phase in double bilayer graphene, Nat. Phys. **13**, 751 (2017).

[38] K. Chen and R. Shindou, Helicoidal excitonic phase in an electron-hole double-layer system, Phys. Rev. B **100**, 035130 (2019).

[39] Y. Zhang and R. Shindou, Dissipationless Spin-Charge Conversion in Excitonic Pseudospin Superfluid, Phys. Rev. Lett. **128**, 066601 (2022).

[40] H. Kroemer, The 6.1 A family (InAs, GaSb, AlSb) and its heterostructures: A selective review, Phys. E **20**, 196 (2004).

[41] A. Perali, D. Neilson, and A. R. Hamilton, High-Temperature Superfluidity in Double-Bilayer Graphene, Phys. Rev. Lett. **110**, 146803 (2013).

[42] S. Conti, A. Perali, F. M. Peeters, and D. Neilson, Multicomponent Electron-Hole Superfluidity and the BCS-BEC Crossover in Double Bilayer Graphene, Phys. Rev. Lett. **119**, 257002 (2017).

[43] P. López Ríos, A. Perali, R. J. Needs, and D. Neilson, Evidence from Quantum Monte Carlo Simulations of Large-Gap Superfluidity and BCS-BEC Crossover in Double Electron-Hole Layers, Phys. Rev. Lett. **120**, 177701 (2018).

[44] W. Y. Liang, Excitons, Phys. Educ. **5**, 226 (1970).

[45] M. Kira, F. Jahnke, and S. W. Koch, Quantum Theory of Secondary Emission in Optically Excited Semiconductor Quantum Wells, Phys. Rev. Lett. **82**, 3544 (1999).

[46] B. Brar, H. Kroemer, J. Ibbetson, and J. H. English, Photoluminescence from narrow InAsAlSb quantum wells, Appl. Phys. Lett. **62**, 3303 (1993).

[47] Y. Wakisaka, T. Sudayama, K. Takubo, T. Mizokawa, M. Arita, H. Namatame, M. Taniguchi, N. Katayama, M. Nohara, and H. Takagi, Excitonic Insulator State in Ta_2NiSe_5 Probed by Photoemission Spectroscopy, Phys. Rev. Lett. **103**, 026402 (2009).